SIAM J. IMAGING SCIENCES
Vol. 2, No. 1, pp. 140–182

On SAR Imaging through the Earth's Ionosphere*

S. V. Tsynkov†

Abstract. We analyze the effect of dispersion of radio waves in the Earth's ionosphere on the performance (image resolution) of spaceborne synthetic aperture radars (SARs). We describe the electromagnetic propagation in the framework of a scalar model for the transverse field subject to weak anomalous dispersion due to the cold plasma. Random contributions to the refraction index are accounted for by the Kolmogorov model of ionospheric turbulence. A key consideration used when analyzing the statistics of waves is normalization of the probability distributions for long propagation distances. The ionospheric phenomena, both deterministic and random, are shown to affect the azimuthal resolution of a SAR sensor stronger than the range resolution; also, the effect of randomness appears weaker than that of the baseline dispersion. Specific quantitative estimates are provided for some typical values of the key parameters. Probing on two carrier frequencies is identified as a possible venue for reducing the ionospheric distortions.

Key words. synthetic aperture radar (SAR), spaceborne radar, ionosphere, dispersion of electromagnetic waves, cold plasma, ionospheric distortions, turbulent fluctuations, geometrical optics, refraction index, range and azimuthal resolution, scattering

AMS subject classifications. 78A05, 78A40, 78A45, 78A46, 78A48, 62P35, 62M40, 78A55

DOI. 10.1137/080721509

1. Introduction.

The dispersion of electromagnetic waves in the Earth's ionosphere is known to impair the performance of synthetic aperture radars (SARs) with their antennas mounted on satellites (as opposed to conventional airborne radars). This issue has received attention in the literature since the inception of the spaceborne SAR technology; see, e.g., [6, 8]. The author of [8] indicates, in particular, that it is difficult to achieve high image resolution for the radars operating in the VHF and UHF frequency bands, i.e., below $1GHz$. The objective of this paper is to quantify some typical ionospheric distortions that have both a deterministic and a stochastic component, and to propose a possible mitigation strategy.

The propagation of high-frequency transverse electromagnetic waves in dilute plasma, e.g., the Earth's ionosphere, is governed by the Klein–Gordon equation:

$$\frac{\partial^2 \boldsymbol{E}_\perp}{\partial t^2} - c^2 \Delta \boldsymbol{E}_\perp + \omega_{\rm pe}^2 \boldsymbol{E}_\perp = \boldsymbol{0}. \tag{1.1}$$

The quantity $\omega_{\rm pe}$ in (1.1) is called the Langmuir frequency, or plasma electron frequency. It

*Received by the editors April 17, 2008; accepted for publication (in revised form) November 11, 2008; published electronically January 30, 2009. This work was supported by the U.S. Air Force Office of Scientific Research (AFOSR) under grant FA9550-07-1-0170.
http://www.siam.org/journals/siims/2-1/72150.html
†Department of Mathematics, North Carolina State University, Box 8205, Raleigh, NC 27695 (tsynkov@math.ncsu.edu, http://www.math.ncsu.edu/~stsynkov).

characterizes temporal responses of the plasma and is given by

$$\omega_{\mathrm{pe}} = \sqrt{\frac{4\pi e^2 N_{\mathrm{e}}}{m_{\mathrm{e}}}}, \tag{1.2}$$

where e and m_{e} are the charge and mass of the electron (fundamental constants), and N_{e} is the electron number density, which depends on many parameters. In the case of a homogeneous plasma, the Langmuir frequency is constant; otherwise, it can vary if the number density N_{e} varies. Typical values of the Langmuir frequency in the Earth's ionosphere range between 3MHz and 15MHz. At the same time, for our key application of interest, which is a spaceborne SAR sensor, typical values of the carrier frequency start at several hundred megahertz (VHF and UHF bands) and go into the gigahertz range (microwave band).

The dispersion relation for the Klein–Gordon equation (1.1) reads as

$$\omega^2 = \omega_{\mathrm{pe}}^2 + c^2 k^2. \tag{1.3}$$

Only the waves with frequencies $\omega > \omega_{\mathrm{pe}}$ can propagate in the plasma. The model of propagation based on the Klein–Gordon equation (1.1) and, accordingly, the dispersion relation (1.3), is known as cold plasma; additional details on its derivation from full Maxwell's equations are provided in Appendix A. Dispersion (1.3) is anomalous; i.e., it is the short waves that are weakly dispersive, whereas the long waves are subject to stronger dispersion. Indeed, the phase and group velocity of the propagation are given by

$$v_{\mathrm{ph}} = c\left(1 + \omega_{\mathrm{pe}}^2/c^2k^2\right)^{\frac{1}{2}} \quad \text{and} \quad v_{\mathrm{gr}} = c\left(1 + \omega_{\mathrm{pe}}^2/c^2k^2\right)^{-\frac{1}{2}}, \tag{1.4}$$

so that the shorter the wave is, i.e., the larger the k is, the closer both velocities are to the nondispersive value $v = c$. In the Cartesian coordinates we can consider (1.1) for individual field components:

$$\frac{\partial^2 E}{\partial t^2} - c^2 \Delta E + \omega_{\mathrm{pe}}^2 E = 0. \tag{1.5}$$

The Fourier transform of (1.5) in time yields

$$\Delta E + \frac{\omega^2}{c^2}\left(1 - \frac{\omega_{\mathrm{pe}}^2}{\omega^2}\right) E = 0. \tag{1.6}$$

The quantity $n(\omega) = \sqrt{1-\omega_{\mathrm{pe}}^2/\omega^2}$ can therefore be interpreted as the refraction index. In the case of a homogeneous plasma it is constant. Otherwise, it can vary in space and, moreover, contain a stochastic component. Randomness can make its way into ω_{pe} because of the turbulence in the ionosphere that causes the fluctuations of N_{e}; see (1.2). The structure of the ionospheric turbulence is complicated and depends on many factors. A good starting point that we adopt for the study is the Kolmogorov-type turbulence.

The imaging of the Earth's surface by a spaceborne SAR is done as follows. The full radar antenna is a synthetic array, which means that the Earth's surface is illuminated by a sequence of pulses transmitted from different locations as the "elementary" antenna mounted on the

satellite travels along the orbit. The received signals that are scattered off the Earth's surface are then processed by means of the matched filtering. In the literature, a common approach to the analysis of synthetic antennas is based on the start-stop approximation (see, e.g., [17]), when one assumes that each individual pulse is emitted, and the corresponding scattered wave is received, while the satellite is at a standstill, after which it moves to the location from which the next pulse is emitted. This approach is well justified for airborne radars when the pulse travel time between the antenna and the target is around $10^{-4}sec$, and the speed of the airplane is about $250m/sec$. The satellite, on the other hand, moves much faster (about $8km/sec$) and flies much higher above the Earth's surface so that for the round-trip travel times of the pulse, which are on the order of several milliseconds, the displacement of the elementary antenna is no longer negligible. It could, in fact, be a few times larger than the antenna size. Moreover, the start-stop approximation does not take into account the Doppler frequency shift, which, again, will be larger for satellites than for airplanes. Nonetheless, the start-stop approximation can still be used for spaceborne SARs, because, as shown in our recent paper [40], the displacement of the antenna during the round-trip travel time of the pulse between the orbit and the ground does not impair the resolution of the image and leads only to the shift of the entire imaged scene. As for the Doppler frequency shift, it does not affect the performance of the radar either as long as it is included in the definition of a matched filter [40]. Note also that the idea of using the matched filters phase-corrected for Doppler is discussed in [12].

In the current paper, we make a number of additional simplifying assumptions:

- We do not consider vector quantities and use the scalar governing equations (1.5) and (1.6) instead of (1.1). We can say that the radar does not measure the polarization of the wave.
- Dispersion relation (1.3) corresponds to the model of cold plasma, in which one takes into account temporal dispersion but disregards spatial dispersion; see Appendix A.
- We also disregard the Ohm conductivity, i.e., assume that the ionospheric plasma behaves like a lossless dielectric.
- We treat the targets as deterministic and disregard all the stochastic effects that may characterize scattering off the Earth's surface. For example, we disregard the noisy component of the received signal caused by roughness of the terrain; see [17].
- We are interested only in obtaining and analyzing the conventional SAR images, as opposed to interferometric images [17]. In other words, we will be looking into the range resolution and azimuthal resolution of the SAR, but will not be looking into its altitude (angle) resolution.
- We use the standard matched filter processing to form a SAR image. We do not include the dechirp-on-receive procedure that is sometimes employed by spotlight SAR systems to stabilize the signal received from the center of the imaged scene [10, section 2.6]. Dechirping is rarely employed by the radars operating in stripmap mode, which is most common for spaceborne imaging.
- We disregard the anisotropy of the plasma due to the magnetic field of the Earth, and hence we do not take into account the Faraday rotation (recall that we do not consider polarization of radio waves).
- We also disregard the effect of the magnetic field of the Earth on the ionospheric

turbulence. The turbulence is always assumed isotropic.

- Both the mean characteristics of the plasma and their fluctuations are strongly affected by the level of solar activity, geographic latitude, time of year, time of day (day/night), etc. For our quantitative estimates, we choose some typical values for all the parameters.
- We disregard multiple scattering at the target(s) and use the Born approximation. On the other hand, we take into account multiple scattering in the ionosphere.
- We temporarily disregard the dispersion of the target. In reality, the target dispersion is of key importance because often this is how the targets are recognized. There are publications in the literature that deal precisely with the dispersion-based characterization of the targets; see, e.g., [29]. Therefore, in the long run we would like to achieve the capability of differentiating between the target dispersion and the ionospheric dispersion that distorts the image.
- We use the approximation of geometrical optics (see [37, Chapters 1–2]) and the geometrical optics perturbations method that allows us to analyze the effect of random turbulent fluctuations of the electron number density in the ionosphere on the resolution of a SAR sensor.

Some of the foregoing physical approximations require certain assumptions about the scaling:

- The approximation of cold plasma holds if the phase speed of electromagnetic waves is much faster than the thermal speed of the electrons in plasma (see Appendix A) (κ is the Boltzmann constant):
$$v_{\mathrm{ph}} \gg \sqrt{\frac{3\kappa T}{2m_{\mathrm{e}}}}.$$
- It is possible to use linearization for computing the waves' travel times and related quantities in plasma when the radar carrier frequency is much higher than the Langmuir frequency:
$$\omega \gg \omega_{\mathrm{pe}}.$$
- Ohm conductivity can be disregarded because we are primarily interested in the regimes for which
$$\omega_{\mathrm{pe}} \gg \nu_{\mathrm{eff}},$$
where ν_{eff} is the effective frequency of collisions between the plasma particles responsible for the onset of conductivity; see Appendix A and [21].
- For the approximation of geometrical optics to hold, the carrier wavelength must be much shorter than the characteristic scale of variations of the mean parameters of the ionosphere (see section 2.1.3),
$$\lambda \ll h_0,$$
and also much shorter than the characteristic scale of turbulent fluctuations of the ionosphere, which we take as the outer scale of turbulence (see (1.12)),
$$\lambda \ll r_0.$$

There is an additional, more subtle, criterion that must be met:

$$\sqrt{\lambda R_0} \ll r_0,$$

where R_0 is the typical propagation distance and the expression on the left-hand side of the previous inequality yields the size of the first Fresnel zone (note that normally $r_0 \ll h_0$).

To characterize the ionospheric turbulence, we write the electron number density as

$$N_{\rm e} = \langle N_{\rm e} \rangle + \mu(\boldsymbol{x}), \tag{1.7}$$

where the angular brackets $\langle \cdot \rangle$ denote the expected value (mean) and μ represents the fluctuations: $\langle \mu \rangle = 0$. In the simplest case of constant $\langle N_{\rm e} \rangle$, $\mu(\boldsymbol{x})$ is a homogeneous and isotropic random field, and its correlation function depends only on the distance $r = |\boldsymbol{x}_1 - \boldsymbol{x}_2|$ and not on the individual locations $\boldsymbol{x}_1$ and $\boldsymbol{x}_2$:

$$V(\boldsymbol{x}_1, \boldsymbol{x}_2) \stackrel{\rm def}{=} \langle \mu(\boldsymbol{x}_1)\mu(\boldsymbol{x}_2) \rangle = V(|\boldsymbol{x}_1 - \boldsymbol{x}_2|) \equiv V(r). \tag{1.8}$$

The spectrum of turbulent fluctuations is defined as the Fourier transform of $V(r)$:

$$\begin{aligned} \widehat{V}(\boldsymbol{q}) &\stackrel{\rm def}{=} \frac{1}{8\pi^3} \iiint_{-\infty}^{\infty} V(\boldsymbol{r}) e^{-i\boldsymbol{q}\boldsymbol{r}} d\boldsymbol{r} = \frac{1}{8\pi^3} \int_0^{\infty} \int_0^{2\pi} \int_0^{\pi} V(r) e^{-iqr\cos\theta} r^2 \sin\theta d\theta d\phi dr \\ &= \frac{1}{4\pi^2} \int_0^{\infty} \int_{-1}^{1} V(r) e^{-iqru} r^2 du dr = \frac{1}{2\pi^2} \int_0^{\infty} \frac{\sin qr}{qr} V(r) r^2 dr \stackrel{\rm def}{=} \widehat{V}(q), \end{aligned} \tag{1.9}$$

where $\boldsymbol{q}$ is the Fourier variable (dual to $\boldsymbol{r} = \boldsymbol{x}_1 - \boldsymbol{x}_2$), $q = |\boldsymbol{q}|$, and the change of variables $u = \cos\theta$ was used when computing the integral (1.9). In the literature, it is often the spectrum that is introduced as the primary characteristic of turbulence. In particular, for the Kolmogorov–Obukhov turbulence, which is typical for the lower ionosphere, the spectrum can be taken in the form suggested in [36, Chapter I]:

$$\widehat{V}(q) = \frac{C}{(1 + q^2/q_0^2)^{\kappa}}, \quad \text{where} \quad \kappa = \frac{11}{6} \quad \text{and} \quad C = \text{const}. \tag{1.10}$$

For the purpose of conducting the derivations, though, it will be more convenient to take a slightly different value of the exponent, $\kappa = 2$, as it yields an exponentially decaying correlation function [32, section 12.1]:

$$V(r) = C\pi^2 q_0^3 e^{-q_0 r}. \tag{1.11}$$

The change from $\kappa = 11/6$ to $\kappa = 2$ in formula (1.10) that leads to the exponential correlation function (1.11) essentially means that we are going to consider only short-range phenomena. The long-range case may present its own subtleties for the analysis, and we leave it as an interesting topic for future study.

The quantity q_0 in formulae (1.10) and (1.11) is inversely proportional to the correlation length:

$$r_0 \stackrel{\rm def}{=} \frac{1}{V(0)} \int_0^{\infty} V(r) dr = \int_0^{\infty} e^{-q_0 r} dr = \frac{1}{q_0}. \tag{1.12}$$

The latter is also referred to as *the outer scale of turbulence;* it can be taken as $r_0 \sim 1km$ according to [2]; the value quoted in [9] is an order of magnitude larger: $r_0 \sim 10km$.

The constant C in formula (1.10) is related to the variance of μ (see [2]):

$$\iiint_{-\infty}^{\infty} \hat{V}(\boldsymbol{q})d\boldsymbol{q} = V(0) = \langle \mu^2 \rangle.$$

Integration of the spectrum (1.10) yields

$$\langle \mu^2 \rangle = \int_0^{\infty} \int_0^{2\pi} \int_0^{\pi} \hat{V}(q) q^2 \sin\theta d\theta d\phi dq = C\pi^{3/2} q_0^3 \frac{\Gamma\left(-\frac{3}{2}+\kappa\right)}{\Gamma(\kappa)},$$

and substituting $\kappa = 2$, we obtain

$$C = \frac{2}{\pi^2} \frac{\langle \mu^2 \rangle}{q_0^3}. \tag{1.13}$$

Magnitude of the fluctuations is also very important. It is typically measured relative to the mean electron density, and the quantity

$$M = \frac{\sqrt{\langle \mu^2 \rangle}}{\langle N_e \rangle} = \frac{\pi}{\sqrt{2}} q_0^{\frac{3}{2}} \frac{\sqrt{C}}{\langle N_e \rangle} \tag{1.14}$$

is assumed altitude independent even if $\langle N_e \rangle$ depends on the altitude. A typical numerical value of M is $5 \cdot 10^{-3}$, and in extreme situations it may reach 10^{-1} [2]. Note that as $\langle N_e \rangle$ becomes altitude dependent so does $\langle \mu^2 \rangle$, which makes the field $\mu(\boldsymbol{x})$ quasi-homogeneous rather than homogeneous [36] (see section 2.1.4).

For the specific examples that we analyze hereafter, we will be choosing the following values of the parameters. A typical mean electron concentration can be taken as $\langle N_e \rangle = 10^6 cm^{-3}$, which yields $\omega_{pe} \approx 9MHz$. The radar carrier frequency will be assumed equal to $1GHz$, which is the lower bound for the microwave band. According to [8], it is very difficult to achieve high resolution of spaceborne SAR images for carrier frequencies under $1GHz$ (if no attempt is made to reduce the distortions due to the ionosphere). We note, though, that many modern radars operate at higher frequencies, often reaching $10GHz$. On the other hand, some other radars operate in the VHF and UHF bands with the wavelength in vacuum $\lambda \gtrsim 1m$ and the frequency ω about several hundred megahertz. Lowering the carrier frequency is very important for certain applications as it may help the signal penetrate deeper into the foliage or soil [27], but it also increases the negative impact of the ionospheric dispersion [8]. Indeed, as we are going to see, the dispersive effects are characterized by the value of the quotient ω_{pe}^2/ω^2. Finally, a typical one-way propagation distance between the satellite and the ground can be taken as $R_0 \approx 1000km$ (in fact, up to $R_0 = 1500km$ with the orbit altitude between $500km$ and $800km$ and the look angle between 20° and 60°).

Let us reemphasize that the ionospheric plasma is dispersive with or without the fluctuations of electron density, because $\langle N_e \rangle \neq 0$. Even when this dispersion is weak ($\omega \gg \omega_{pe}$), synthetic aperture imaging through the ionosphere is not completely identical to the case $\omega_{pe} = 0$ discussed in [11]. Indeed, the image is formed by applying a matched filter to the

field received by the antenna; see section 2.1 or [17] for more detail. This procedure is also related to the time-reversal imaging; see, e.g., [7]. The matched filter that would be optimal for the propagation governed by (1.5) will differ from that used in the case $\omega_{\rm pe} = 0$, when (1.5) transforms into the d'Alembert equation. A methodology for building the matched filters that takes into account the dispersion of waves was proposed in [13]. The approach of [13] assumes, however, that all the parameters that quantify the dispersion are known. Unfortunately, this cannot be considered the case for the Earth's ionosphere, which is a very "lively" medium with its key characteristics, such as $N_{\rm e}$, changing rapidly, so that no precise values can be predicted at a given moment of time and given location. Hence, liveliness of the ionosphere will limit the applicability of the modified matched filters that employ the models of dispersion with known parameters, even if the latter are as simple as (1.3). Note also that when imaging through a dispersive layer, there is room for optimization not only of the matched filters, but also of the waveforms emitted by the radar; see [3].

Among other publications in the literature that address the issue of SAR performance in the presence of the Earth's ionosphere we mention work [2] that discusses both the deterministic and stochastic aspects of the propagation of electromagnetic waves in the ionospheric plasma, work [18] that focuses on the issues related to Faraday rotation and the corresponding calibration strategies, and work [25] that discusses only the homogeneous plasma and, again, emphasizes the need for calibration. Work [16] also discusses only the ionosphere with uniform electron concentration, but estimates the distortions of a SAR image at a rather low carrier frequency of $250 MHz$ with the respectively high bandwidth of 100 MHz. The authors of [23] analyze the homogeneous ionosphere and determine that the distortions are greater for lower frequencies, and that the adverse effect of the ionospheric dispersion is worse for the azimuthal resolution than for the range resolution of a SAR sensor. In [28], the findings of [23] are extended to the inhomogeneous case using a numerical technique. In work [34], the turbulence-induced phase fluctuations along the synthetic antenna were simulated numerically following a given statistics, and radar performance was assessed from the results of simulations. We also mention two closely related papers, [9, 20], in which several methodologies are discussed for mitigating the random phase errors based on the image postprocessing. The effect of deterministic dispersion on the quality of the SAR images is not addressed in [9, 20]. The authors of [26] use the measured parameters of the ionosphere from two independent experiments to analyze the performance of a space-based radar. Finally, work [42] surveys the literature and provides a comprehensive review of both the deterministic and stochastic ionospheric effects on a spaceborne SAR sensor.

While many publications in the literature discuss the deterioration of SAR performance due to the ionosphere, relatively few papers offer any compensation techniques. In that regard, we should mention the U.S. Patent [4] that proposes to estimate the effective ionospheric conditions by measuring the varying group delay (signal slowdown induced by the ionosphere as it depends on the frequency) in multiple subbands of the operating frequency range. The estimated parameters of the ionosphere can subsequently be used for modifying the matched filter of the SAR.

In the rest of the current paper, we first provide quantitative estimates of how the ionospheric dispersion affects the performance of a spaceborne SAR if the conventional matched filter is employed. Next, we propose a strategy of how one can potentially modify the standard

"nondispersive" matched filtering algorithm to compensate for the ionospheric dispersion, and outline a possible pathway toward implementing the corresponding modifications.

2. Resolution. Resolution of a radar is its ability to distinguish between separate targets. It is typically determined by the minimum distance between two point targets (delta-type) that the radar can still tell apart. Accordingly, there are different types of resolution that characterize the performance of a SAR system. Those are the range resolution (in the direction perpendicular to the flight track), azimuthal resolution (along the flight track), and altitude resolution. Altitude is measured only by the interferometric SAR (IFSAR) sensors that employ two antennas with slightly different observation angles (see [17]), and we will not consider that.

The ionospheric distortions that impair the resolution of a SAR sensor are due to the deterministic dispersion of radio waves in the ionosphere, as well as to random turbulent fluctuations of the electron number density. Our analysis shows that both factors tend to hamper the azimuthal resolution more strongly than they hamper the range resolution. This observation correlates with other findings in the literature [2].

Let us also note that, as shown in [5, 7], synthetic aperture images may also show good range resolution in a different setting that involves the propagation of acoustic waves with random speed but no dispersion. However, the range resolution deteriorates if the frequency decoherence in the medium becomes rapid. Further analysis of range resolution in synthetic aperture imaging through the media with random propagation speed can be found in [19], where large perturbations of the travel time are also discussed.

In what follows, we adopt the framework and some of the notations of [11]. The antenna emits a series of pulses as the satellite moves along the orbit. Each pulse is a linear upchirp of the form

$$P(t) = A(t)e^{i\omega_0 t}, \quad \text{where} \quad A(t) = \chi_\tau(t)e^{i\alpha t^2}. \tag{2.1}$$

In formula (2.1), $\chi_\tau(t)$ is the indicator function of the interval of duration τ:

$$\chi_\tau(t) = \begin{cases} 1, & t \in [-\tau/2, \tau/2], \\ 0 & \text{otherwise}, \end{cases}$$

and $\alpha = B/(2\tau)$, where B is the bandwidth of the chirp. Accordingly, the instantaneous frequency of the chirp is given by

$$\omega(t) = \omega_0 + \frac{Bt}{\tau}, \quad t \in [-\tau/2, \tau/2], \tag{2.2}$$

where ω_0 is the center carrier frequency. The modulating function $A(t)$ in formula (2.1) is slowly varying. A typical duration of the pulse in actual SAR systems may be $\tau \sim 5{\cdot}10^{-5} sec$, a typical interval between two consecutive pulses is $\sim 5 \cdot 10^{-4} sec$, and the bandwidth in formula (2.2) is $B \sim 10 MHz$ (it may be higher).

When analyzing the performance of a radar, one commonly introduces and studies the point spread function, which is basically the image of one point target. In the case of a synthetic antenna, the performance is improved by superimposing the information from multiple scattered pulses. Then, one introduces and studies the generalized ambiguity function of a

radar obtained by summing up the individual point spread functions. Let $\boldsymbol{x}^n$ be the location of the antenna at the time t_n when pulse number n is emitted, $\boldsymbol{z}$ be the location of a point target, and $\boldsymbol{y}$ be the location of a reference point scatterer (i.e., a probing location). According to [11], the generalized ambiguity function of a synthetic antenna is given by the following expression:

$$
\begin{aligned}
W(\boldsymbol{y},\boldsymbol{z}) &= \sum_n w(\boldsymbol{z}-\boldsymbol{x}^n)\int \overline{P(t-t_n-2|\boldsymbol{y}-\boldsymbol{x}^n|/c)}P(t-t_n-2|\boldsymbol{z}-\boldsymbol{x}^n|/c)dt \\
&= \sum_n w(\boldsymbol{z}-\boldsymbol{x}^n)\int \overline{A(t-t_n-2|\boldsymbol{y}-\boldsymbol{x}^n|/c)}e^{-i\omega_0(t-t_n-2|\boldsymbol{y}-\boldsymbol{x}^n|/c)} \\
&\qquad\qquad A(t-t_n-2|\boldsymbol{z}-\boldsymbol{x}^n|/c)e^{i\omega_0(t-t_n-2|\boldsymbol{z}-\boldsymbol{x}^n|/c)}dt.
\end{aligned}
\tag{2.3}
$$

The overbar in formula (2.3) denotes complex conjugation (time reversal). Each term in the sum has two factors under the integral. The factor $P(\,\cdot\,)$ is proportional to the actual field received by the antenna after the pulse has been emitted and sent back by the delta-type scattering potential concentrated at $\boldsymbol{z}$. This form of the scattered field corresponds to the free unobstructed propagation between the antenna and the target, and is obtained by solving the d'Alembert equation using retarded potentials and the first Born approximation for scattering. In doing so, one also takes into account that $A(\,\cdot\,)$ varies slowly compared to the fast oscillation with the frequency ω_0; see [11]. The quantity $2|\boldsymbol{z}-\boldsymbol{x}^n|/c$ is the round-trip travel time in vacuum between the antenna at $\boldsymbol{x}^n$ and the target at $\boldsymbol{z}$. The received field is matched against the second factor, $\overline{P(\,\cdot\,)}$, which is proportional to the complex conjugate of the signal scattered by the reference delta scatterer at $\boldsymbol{y}$. Similarly, the quantity $2|\boldsymbol{y}-\boldsymbol{x}^n|/c$ is the round-trip travel time in vacuum between the antenna at $\boldsymbol{x}^n$ and the reference location $\boldsymbol{y}$. The idea behind processing the received field with the matched filter is to try to make the ambiguity function $W(\boldsymbol{y},\boldsymbol{z})$ as close to the delta function $\delta(\boldsymbol{y}-\boldsymbol{z})$ as possible so that when imaging the terrain by moving the reference location $\boldsymbol{y}$, the image would have a sharp peak at the location of the actual target $\boldsymbol{z}$ and would be zero or very small elsewhere. In reality, the actual delta function $\delta(\boldsymbol{y}-\boldsymbol{z})$ is never achieved, but the peak can be considerably sharpened by summing over n, i.e., over the elements of the synthetic antenna.

The quantity $w(\boldsymbol{z}-\boldsymbol{x}^n)$ in formula (2.3) denotes the directivity pattern of the antenna on the satellite. It determines the range of the summation and can be approximated as follows. Let $\lambda=\frac{2\pi c}{\omega_0}$ denote the wavelength, and let L be the size of the antenna on the satellite in the direction of the orbit. Then, the angular width of the antenna beam is approximately equal to $\frac{2\lambda}{L}$, provided that $\lambda \ll L$; see Appendix B. Let us use the subscript "1" for the coordinate along the orbit (assumed locally straight). Then, for the angle ϕ between the direction $\boldsymbol{z}-\boldsymbol{x}^n$ and the normal to the orbit that would belong to the same plain as $\boldsymbol{z}-\boldsymbol{x}^n$ and the orbit itself, we can write (R_0 is the distance to the ground along this normal)

$$
\tan\phi=\frac{z_1-x_1^n}{R_0}.
$$

The directivity function $w(\boldsymbol{z}-\boldsymbol{x}^n)$ is equal to 1 if the given direction $\boldsymbol{z}-\boldsymbol{x}^n$ is within the

antenna beam, and it is equal to zero otherwise:

$$w(\boldsymbol{z}-\boldsymbol{x}^n)=\begin{cases}1 & \text{if } -\frac{\lambda}{L}\le\phi\le\frac{\lambda}{L},\\ 0 & \text{if } \phi<-\frac{\lambda}{L} \text{ or } \phi>\frac{\lambda}{L}.\end{cases}$$

Hence, using the approximation $\tan\phi\approx\phi$ for small ϕ, we have

$$w(\boldsymbol{z}-\boldsymbol{x}^n)=\begin{cases}1 & \text{if } z_1-\frac{\lambda R_0}{L}\le x_1^n\le z_1+\frac{\lambda R_0}{L},\\ 0 & \text{if } x_1^n<z_1-\frac{\lambda R_0}{L} \text{ or } x_1^n>z_1+\frac{\lambda R_0}{L}.\end{cases} \tag{2.4}$$

The range of the summation in (2.3) is therefore defined by taking into account only those $\boldsymbol{x}^n$ for which $w(\boldsymbol{z}-\boldsymbol{x}^n)\neq 0$ or, equivalently, for which $\boldsymbol{z}$ stays in the beam; see (2.4). Let Δx_1 be the distance along the orbit between the successive emissions of pulses. Let us also take $z_1=0$, which does not imply any loss of generality. Then, the inequality $-\frac{\lambda R_0}{L}\le x_1^n\le\frac{\lambda R_0}{L}$ translates into $-\frac{N}{2}\le n\le\frac{N}{2}$, where $N=[\frac{2\lambda R_0}{\Delta x_1 L}]$ and $[\,\cdot\,]$ stands for the integer part. Consequently, we recast (2.3) as

$$\begin{aligned}W(\boldsymbol{y},\boldsymbol{z})=\sum_{-N/2}^{N/2}\int&\overline{A(t-t_n-2|\boldsymbol{y}-\boldsymbol{x}^n|/c)}e^{2i\omega_0|\boldsymbol{y}-\boldsymbol{x}^n|/c}\\ &\times A(t-t_n-2|\boldsymbol{z}-\boldsymbol{x}^n|/c)e^{-2i\omega_0|\boldsymbol{z}-\boldsymbol{x}^n|/c}dt.\end{aligned} \tag{2.5}$$

Next, we change the variable from $t-t_n$ to t in each term of the sum (2.5) and realize that neither $\overline{A(t-2|\boldsymbol{y}-\boldsymbol{x}^n|/c)}$ nor $A(t-2|\boldsymbol{z}-\boldsymbol{x}^n|/c)$ depends on n explicitly, except for the dependence via $\boldsymbol{x}^n$. The latter is weak, because if R_0 is large, then both $|\boldsymbol{y}-\boldsymbol{x}^n|$ and $|\boldsymbol{z}-\boldsymbol{x}^n|$ are slowly varying functions of $\boldsymbol{x}^n$, while A is another slowly varying function on top of it. Consequently, the factors $\bar{A}$ and A can be taken out of the sum (2.5), and $\boldsymbol{x}^n$ can be replaced by $\boldsymbol{x}^0$ for definiteness, which yields

$$W(\boldsymbol{y},\boldsymbol{z})\approx\left(\underbrace{\int\overline{A(t-2|\boldsymbol{y}-\boldsymbol{x}^0|/c)}A(t-2|\boldsymbol{z}-\boldsymbol{x}^0|/c)dt}_{W_R(\boldsymbol{y},\boldsymbol{z})}\right)\left(\underbrace{\sum_{-N/2}^{N/2}e^{2i\omega_0(|\boldsymbol{y}-\boldsymbol{x}^n|/c-|\boldsymbol{z}-\boldsymbol{x}^n|/c)}}_{W_A(\boldsymbol{y},\boldsymbol{z})}\right). \tag{2.6}$$

Formula (2.6) indicates that the generalized ambiguity function gets approximately decomposed into the product of the range factor,

$$W_R(\boldsymbol{y},\boldsymbol{z})=\int\overline{A(t-2|\boldsymbol{y}-\boldsymbol{x}^0|/c)}A(t-2|\boldsymbol{z}-\boldsymbol{x}^0|/c)dt, \tag{2.7}$$

and the azimuthal factor,

$$W_A(\boldsymbol{y},\boldsymbol{z})=\sum_{n=-N/2}^{N/2}e^{2i\omega_0(|\boldsymbol{y}-\boldsymbol{x}^n|/c-|\boldsymbol{z}-\boldsymbol{x}^n|/c)}. \tag{2.8}$$

We will see that W_R of (2.7) and W_A of (2.8) do indeed control the range and azimuthal resolution, respectively.

2.1. Range resolution. In the ideal case of no ionosphere, computation of the range ambiguity factor W_R of (2.7) in [11] (see also [17]) yields the following expression for the range resolution of a SAR:

$$\Delta R = \frac{2\pi c}{B}. \tag{2.9}$$

The quantity ΔR defined by (2.9) is the minimum distance in the direction perpendicular to the satellite flight track, at which the system can still tell a pair of different point targets apart.

2.1.1. Homogeneous ionosphere. In reality, however, the signal between the antenna and the target propagates through the Earth's ionosphere. The ionosphere makes the propagation speed depend on the frequency (see (1.4)) and hence *changes the waves' travel times between the antenna and the target(s).* To analyze the effect of these distortions on the range resolution, we will use an approach which is often employed for the analysis of dispersive propagation; see, e.g., [24] and also [39, section 3.4]. This approach assumes that the pulse (2.1) can be artificially split into a number of parts that correspond to different instantaneous frequencies (2.2), and that these parts will travel with the group velocities that vary accordingly. This technique is not quite equivalent to performing a full-fledged analysis with the help of the Fourier transform,[1] but it is more intuitive and the results are far more apparent. Hereafter, we will be assuming that the signal is fairly narrow band, $B \ll \omega_0$, which is typical for many actually operating SAR sensors; see [17]. We will also be employing the high-frequency approximation, $\omega_{\rm pe} \ll \omega_0$, which is perfectly reasonable for most applications and which implies (cf. formula (1.4))

$$v_{\rm gr} \approx c\left(1 - \frac{\omega_{\rm pe}^2}{2c^2k^2}\right) = c\left(1 - \frac{\omega_{\rm pe}^2}{2(\omega^2 - \omega_{\rm pe}^2)}\right) \approx c\left(1 - \frac{\omega_{\rm pe}^2}{2\omega^2}\right), \tag{2.10}$$
$$\text{where} \quad \omega \in [\omega_{\min}, \omega_{\max}] \equiv [\omega_0 - B/2, \omega_0 + B/2].$$

Note that as of yet the ionosphere is assumed homogeneous, $\omega_{\rm pe} = \text{const}$. Later, we will also analyze the case when the electron number density $N_{\rm e}$, and hence the Langmuir frequency $\omega_{\rm pe}$, depend on the altitude.

Given the variation of the group velocity (2.10), we can see that the pulse (2.1) gets dilated during the time that it travels back and forth between the satellite $\boldsymbol{x}^n$ and the target $\boldsymbol{z}$. Accordingly, there are a new (longer) pulse duration τ' and a new pulse rate α':

$$A'(t) = \chi_{\tau'}(t)e^{i\alpha' t^2}. \tag{2.11}$$

The quantity $\tau' = \tau + \delta\tau$ in formula (2.11) is determined by the natural consideration that the highest frequency $\omega_{\max}$ travels the fastest and the lowest frequency $\omega_{\min}$ travels the slowest. Hence, denoting $R_{\boldsymbol{z}} = |\boldsymbol{z} - \boldsymbol{x}^0|$, taking into account formula (2.10), and using Taylor's

[1] This is primarily because the full spectrum of the signal (2.1) contains other frequencies besides $\omega \in [\omega_0 - B/2, \omega_0 + B/2]$.

expansion, we find

$$\begin{aligned}\delta\tau &= \frac{2R_{\boldsymbol{z}}}{v_{\rm gr}(\omega_{\min})} - \frac{2R_{\boldsymbol{z}}}{v_{\rm gr}(\omega_{\max})} = \frac{2R_{\boldsymbol{z}}}{v_{\min}} - \frac{2R_{\boldsymbol{z}}}{v_{\max}} \\ &= \frac{2R_{\boldsymbol{z}}(v_{\max}-v_{\min})}{v_{\max}v_{\min}} \approx 2R_{\boldsymbol{z}}c\left[\left(1-\frac{\omega_{\rm pe}^2}{2\omega_0^2}\left(1-\frac{B}{\omega_0}\right)\right) - \left(1-\frac{\omega_{\rm pe}^2}{2\omega_0^2}\left(1+\frac{B}{\omega_0}\right)\right)\right] \\ &\times \left[c^2\left(1-\frac{\omega_{\rm pe}^2}{2\omega_0^2}\left(1-\frac{B}{\omega_0}\right)\right)\cdot\left(1-\frac{\omega_{\rm pe}^2}{2\omega_0^2}\left(1+\frac{B}{\omega_0}\right)\right)\right]^{-1} \approx \frac{2R_{\boldsymbol{z}}}{c}\frac{\omega_{\rm pe}^2}{\omega_0^2}\frac{B}{\omega_0}.\end{aligned} \tag{2.12}$$

The quantity α' in (2.11) is the new pulse rate (cf. formula (2.2)):

$$\begin{aligned}&\omega(t) = \omega_0 + \frac{Bt}{\tau'} \equiv \omega_0 + 2\alpha' t, \quad t\in[-\tau'/2,\tau'/2], \\ &\alpha' = \frac{B}{2\tau'} \approx \frac{B}{2\tau}\left(1-\frac{\delta\tau}{\tau}\right) = \alpha+\delta\alpha, \quad \delta\alpha = -\frac{B\delta\tau}{2\tau^2}.\end{aligned} \tag{2.13}$$

Then, introducing another similar notation, $R_{\boldsymbol{y}} = |\boldsymbol{x}^0 - \boldsymbol{y}|$, and using expression (2.11) rather than (2.1) in the capacity of the received signal in formula (2.7), we can rewrite the latter as follows:

$$W_R'(\boldsymbol{y},\boldsymbol{z}) = \int \overline{A(t-2R_{\boldsymbol{y}}/c)}A'(t-2R_{\boldsymbol{z}}/v_0)dt, \tag{2.14}$$

where

$$v_0 \approx c\left(1-\frac{\omega_{\rm pe}^2}{2(\omega_0^2-\omega_{\rm pe}^2)}\right) \approx c\left(1-\frac{\omega_{\rm pe}^2}{2\omega_0^2}\right)$$

is the group velocity that corresponds to the center pulse frequency ω_0; see formula (2.10). We emphasize that in formula (2.14) and further on, the actual received field, which is subject to the ionospheric distortions, is "matched" against the filter based on the model of unobstructed propagation. The resulting mismatch is precisely the reason for all the distortions of the image that we discuss in the paper. The filter, however, cannot be adjusted easily because the relevant parameters of the ionosphere are not known ahead of time. A possible approach to adjusting the filter is discussed in section 3.

To estimate the effect of pulse dilation (2.12) on the range resolution we need to evaluate integral (2.14):

$$\begin{aligned}W_R'(\boldsymbol{y},\boldsymbol{z}) &= \int_{\max\{-\tau/2+2R_{\boldsymbol{y}}/c,\,-\tau'/2+2R_{\boldsymbol{z}}/v_0\}}^{\min\{\tau/2+2R_{\boldsymbol{y}}/c,\,\tau'/2+2R_{\boldsymbol{z}}/v_0\}} e^{-i\alpha(t-2R_{\boldsymbol{y}}/c)^2}e^{i\alpha'(t-2R_{\boldsymbol{z}}/v_0)^2}dt \\ &= e^{4i(\alpha'R_{\boldsymbol{z}}^2/v_0^2-\alpha R_{\boldsymbol{y}}^2/c^2)}\int_{\max\{-\tau/2+2R_{\boldsymbol{y}}/c,\,-\tau'/2+2R_{\boldsymbol{z}}/v_0\}}^{\min\{\tau/2+2R_{\boldsymbol{y}}/c,\,\tau'/2+2R_{\boldsymbol{z}}/v_0\}} e^{i(\alpha'-\alpha)t^2}e^{4i(\alpha R_{\boldsymbol{y}}/c-\alpha' R_{\boldsymbol{z}}/v_0)t}dt.\end{aligned} \tag{2.15}$$

Details of the calculation are provided in Appendix C, and here we summarize the results. Initially, the quadratic term in the exponent under the integral on the right-hand side of (2.15) is disregarded because it is small. This yields (see formula (C.3))

$$W_R'(\boldsymbol{y},\boldsymbol{z}) \propto \tau{\rm sinc}\left(2[(R_{\boldsymbol{y}}-R_{\boldsymbol{z}})(\alpha'/c)+R_{\boldsymbol{z}}\alpha'(1/c-1/v_0)]\tau\right). \tag{2.16}$$

The sinc function, $\operatorname{sinc} x \stackrel{\text{def}}{=} \frac{\sin x}{x}$, that appears in formula (2.16) is often encountered when analyzing the radar resolution [17, 11]. In fact, this function is what one actually obtains instead of the ideal delta function. The maximum of the sinc is normally attained when the reference position $\boldsymbol{y}$ coincides with the location of the target $\boldsymbol{z}$. However, on the right-hand side of formula (2.16) the argument of the sinc function is not equal to zero when $R_{\boldsymbol{y}} = R_{\boldsymbol{z}}$, i.e., when the reference point $R_{\boldsymbol{y}}$ coincides with the given location of the target $R_{\boldsymbol{z}}$. Instead, the argument of the $\operatorname{sinc}(\,\cdot\,)$ is shifted by $R_{\boldsymbol{z}}\alpha'(1/c - 1/v_0)\tau$, which means that the maximum is attained elsewhere. This implies that the standard matched filter processing of the received SAR signal [11] may yield a somewhat shifted absolute position of the target when the ionosphere is present. The corresponding shift is obtained by requiring that the argument of the $\operatorname{sinc}(\,\cdot\,)$ in formula (2.16) be equal to zero, which yields

$$R_{\boldsymbol{y}} - R_{\boldsymbol{z}} = R_{\boldsymbol{z}}(1/v_0 - 1/c)c. \tag{2.17}$$

The shift (2.17) is obviously due to the difference between the travel time in the ionosphere (speed v_0) and the travel time in vacuum (speed c).

However, regarding the resolution of the SAR system, i.e., its ability to distinguish between different targets, what matters is the width of the main lobe of the sinc function. Two targets separated by a distance larger than this width can be distinguished from one another. For the semiwidth we find from formula (2.16), $2(R_{\boldsymbol{y}} - R_{\boldsymbol{z}})\alpha'\tau/c = \pi$. Then, using the expression from (2.13) for the modified pulse rate α' we have (cf. formula (2.9))

$$\Delta R = \frac{2\pi c}{B}\frac{\tau'}{\tau} = \frac{2\pi c}{B}\left(1 + \frac{\delta\tau}{\tau}\right). \tag{2.18}$$

Formula (2.18) implies that the deterioration of the range resolution of a SAR sensor due to the pulse dilation is, in fact, minute. For the typical parameters of section 1, including $\tau \sim 5\cdot 10^{-5} sec$, we obtain a relative change in the resolution of about 0.01% compared to (2.9) (provided that $\delta\tau B/8$ is still small so that the zeroth order Taylor formula can be applied to the first exponential function under the integral (C.1)). We also realize that even for a stronger dispersion (lower values of ω_0) the extent of deterioration in the range resolution will remain acceptable. For example, if $\omega_0 = 300 MHz$ ($\lambda = 1m$) and all other parameters stay the same, we will have $\delta\tau/\tau \approx 0.4\%$. In this case, though, instead of (C.2) we obtain $\delta\tau B \approx 4\pi$.

If the quadratic term in the exponent under the integral on the right-hand side of (2.15) is brought back, then the integral cannot be expressed via elementary functions, but it can be evaluated using the error function erf; see Appendix C. The resulting function $W'_R(\boldsymbol{y}, \boldsymbol{z})$ is complex valued, and one needs to study the behavior of its modulus $|W'_R(\boldsymbol{y}, \boldsymbol{z})|$ in order to analyze the range resolution. It is shown in Appendix C that $|W'_R(\boldsymbol{y}, \boldsymbol{z})|$ reaches its maximum and minimum value at the exact same locations at which the corresponding sinc reaches its maximum value and the first zero, respectively. More precisely, the maximum of $|W'_R(\boldsymbol{y}, \boldsymbol{z})|$ is attained when $R_{\boldsymbol{y}}/c - R_z/v_0 = 0$, and its value is

$$|W'_R(\boldsymbol{y}, \boldsymbol{z})|\Big|_{R_{\boldsymbol{y}}/c - R_z/v_0 = 0} = \tau\left(1 - \frac{\delta\alpha^2\tau^4}{180} + \mathcal{O}(\delta\alpha^3\tau^6)\right),$$

which is very close to $\max \tau \mathrm{sinc}\,[2\alpha'(R_{\boldsymbol{y}}/c - R_z/v_0)] = \tau$ because, for the typical parameters that we have chosen, $\delta\alpha^2\tau^4/180 \sim 2 \cdot 10^{-4}$. The minimum of $|W_R'(\boldsymbol{y}, \boldsymbol{z})|$ is attained for $4\alpha'(R_{\boldsymbol{y}}/c - R_z/v_0) = 2\pi/\tau$, and its value is (see formula (C.5))

$$|W_R'(\boldsymbol{y}, \boldsymbol{z})|\Big|_{4\alpha'(R_{\boldsymbol{y}}/c - R_z/v_0) = \frac{2\pi}{\tau}} = \tau \frac{\delta\alpha\tau^2}{2\pi^2}\left(1 + \mathcal{O}(\delta\alpha\tau^2)\right) \approx \tau \cdot 10^{-2}. \tag{2.19}$$

Thus, we can redefine the width of the main lobe of the ambiguity function $|W_R'|$ as twice the distance between its central maximum and the first minimum, as opposed to twice the distance between the central maximum and the first zero $4\alpha'(R_{\boldsymbol{y}}/c - R_z/v_0) = 2\pi/\tau$. Having done that, we conclude that bringing the factor $e^{i(\alpha'-\alpha)u^2}$ back into the integral (2.15) does not affect this newly redefined quantity. In other words, technically speaking, the range resolution stays the same as before. What does get changed, though, is the sharpness of the minimum, which is directly related to the contrast of the image. For the specific parameters we have chosen, the value of the minimum at $4\alpha'(R_{\boldsymbol{y}}/c - R_z/v_0) = 2\pi/\tau$ is about 1% of that of the central maximum; see formula (2.19).

It should be emphasized, however, that even though the (redefined) width of the main lobe of $|W_R'|$ may remain unaffected, the deteriorating contrast may still impair the actual resolution of the radar. Consider, say, a hypothetical ultimately unfavorable scenario when the ratio of maximum to minimum is $\mathcal{O}(1)$. Then, the resolution will obviously be lost. Therefore, the notion of resolution itself may need to be redefined to accommodate the new considerations that appear in the context of dispersive propagation. Apparently there could be alternative ways of doing that, and we leave this question for future study.

2.1.2. Removing the shift. The shift in the actual range of the target (2.17), which characterizes the image obtained by standard matched filtering can, in fact, be removed. To do so, one needs to probe the terrain (and hence the ionosphere) on two different frequencies. We note that the idea of two frequencies has been discussed previously, although in a somewhat different context related to Faraday rotation [1]. Let ω_1 be another center carrier frequency that is well separated from ω_0, and let v_1 be the corresponding group speed given by formula (1.4) or by the approximate formula (2.10). Then, similarly to (2.17) we can write

$$R_{\boldsymbol{y}}^{(1)} - R_{\boldsymbol{z}} = R_{\boldsymbol{z}}(1/v_1 - 1/c)c. \tag{2.20}$$

Equations (2.17) and (2.20) form a system with two unknowns, ω_{pe} and $R_{\boldsymbol{z}}$, whereas $R_{\boldsymbol{y}}$ and $R_{\boldsymbol{y}}^{(1)}$ provide the known input, i.e., the ranges for a particular unknown target that the radar measures on two chosen frequencies. The accurate value of $R_{\boldsymbol{z}}$ can thus be reconstructed by solving this system. We emphasize that this approach does not require a priori knowledge of ω_{pe}, which is very convenient because the Langmuir frequency is affected by too many factors and is never known precisely. Moreover, the same approach will also work for the inhomogeneous case, when ω_{pe} depends on the altitude and travel times are obtained by integration (see the end of section 2.1.3). In fact, not only does this approach not require the knowledge of the plasma quantities ahead of time, but it recovers those quantities as well, as a part of the solution of the same system. Our idea of how one can possibly reduce the ionospheric distortions on the spaceborne SAR images (see section 3) is centered precisely around this consideration.

2.1.3. Inhomogeneous ionosphere. In this section, we assume that the electron number density N_e and hence the Langmuir frequency ω_{pe} depend on the altitude h. To analyze this case, we basically need to repeat the analysis of section 2.1.1, but replace the expression R_z/v_0 for the travel time between the antenna and the target in formula (2.14) by the appropriate expression for the inhomogeneous ionosphere. To obtain the latter, we should take into account two factors: first, that the propagation speed will vary along the ray trajectory; and second, that this trajectory will be a curve rather than a straight line because of the variation in the refraction index.

Let x denote the horizontal coordinate (along the Earth's surface). Then, with no loss of generality, we can assume that (x, h) is the propagation plane for the waves. Hereafter, we will assume that $N_e = N_e(h)$ but, at the same time, that N_e does not depend on x. A typical dependence of the electron number density on the altitude h is nonmonotonic. The maximum is reached in the F-layer at somewhat over $200km$ above the Earth's surface, and the characteristic scale h_0 of the variations of N_e is on the order of tens of kilometers;[2] see [21, Chapter VI]. Since obviously $h_0 \gg \lambda$, where λ denotes any wavelength that may be of interest for SAR applications, we can indeed use the geometrical optics to determine the wave trajectories.

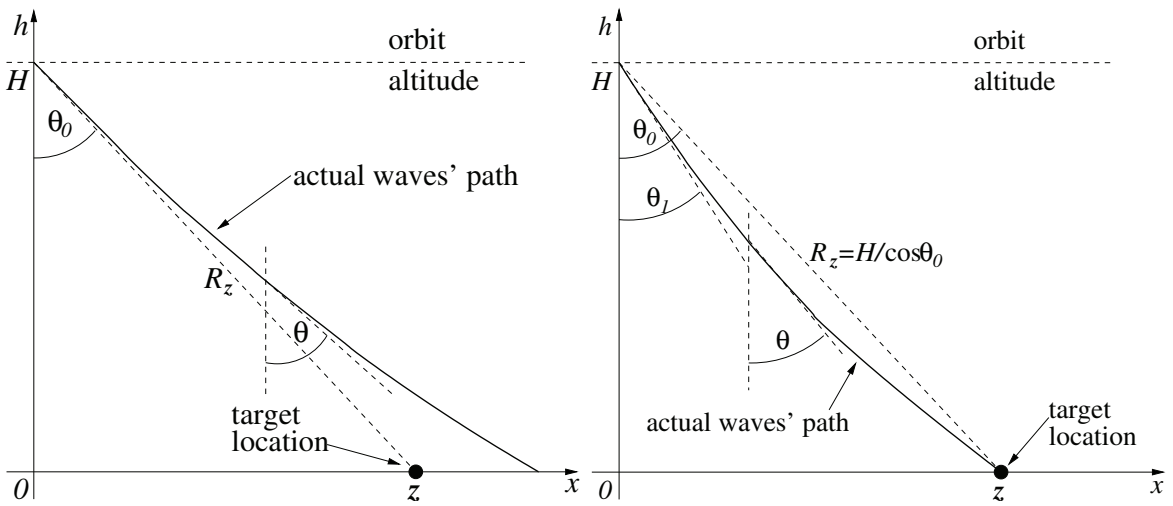

(a) With no correction of the look angle.

(b) With the correction of the look angle.

Figure 1. *Schematic waves' travel paths between the antenna and the target in the inhomogeneous ionosphere.*

Suppose that the antenna is positioned at $x = 0$ and has altitude H above the Earth. It sends a signal toward the target z on the ground (see Figure 1(a)) so that the look angle to the target is equal to θ_0 and, as such, $R_z = H/\cos\theta_0$. As the medium we are considering is lossless (collisionless dilute plasma with no Ohm conductivity; see section 1), its electric

[2] These are regular variations of the mean electron density, as opposed to turbulent fluctuations considered in section 2.1.4.

permittivity is real:

$$\epsilon(h) = 1 - \frac{\omega_{\rm pe}^2(h)}{\omega^2}, \quad \text{where} \quad \omega_{\rm pe}^2(h) = \frac{4\pi e^2 N_{\rm e}(h)}{m_{\rm e}},$$

and we can write Snell's law in the continuous form [21, section 19] as follows:

$$n(h)\sin\theta(h) = n(H)\sin\theta_0, \tag{2.21}$$

where the refraction index is given by

$$n(h) = \sqrt{\epsilon(h)} = \sqrt{1 - \frac{\omega_{\rm pe}^2(h)}{\omega^2}}.$$

Note that, technically speaking, formula (2.21) holds only for plane waves. The angle $\theta(h)$ in formula (2.21) is the angle that the tangent to the wave trajectory at a given altitude h makes with the negative ordinate axis; see Figure 1(a). Then, along the trajectory we can write with the help of (2.21)

$$\frac{dx}{dh} = -\tan\theta(h) = -\frac{n(h)\sin\theta(h)}{n(h)\cos\theta(h)} = -\frac{n(H)\sin\theta_0}{n(h)\cos\theta(h)} = -\frac{n(H)\sin\theta_0}{\sqrt{n^2(h) - n^2(H)\sin^2\theta_0}}. \tag{2.22}$$

Hence, the actual trajectory can be obtained by integrating (2.22):

$$x(h) = \int_H^h \frac{dx}{dh}dh = \int_h^H \frac{n(H)\sin\theta_0}{\sqrt{n^2(h) - n^2(H)\sin^2\theta_0}}dh. \tag{2.23}$$

The shape of the curve (2.23) is determined by the profile of the refraction index $n = n(h)$, and the curve is also parameterized by the look angle θ_0 at the location of the antenna. Note that the shape shown in Figure 1(a) is only schematic, and since the actual profile $n = n(h)$ is nonmonotonic the real curve $x = x(h)$ can look more "bizarre." Note also that with no variation in the refraction index, $n(h) \equiv n(H)$, formula (2.23) yields the straight line between the antenna and the target:

$$x(h) = (H - h)\tan\theta_0. \tag{2.24}$$

As, however, the refraction index is not constant, the ray that originates at the antenna under the look angle θ_0 will not, generally speaking, hit the target; see Figure 1(a). Consequently, a correction to the initial look angle is needed to make sure that the wave trajectory that originates at the antenna under the new angle θ_1 would come precisely to the target; see Figure 1(b).

The actual shape of the trajectory, as well as the waves' travel time along this trajectory, is computed in Appendix D. Here we provide only the final expression for the travel time (see formula (D.7)):

$$T = \frac{R_z}{c}\left\{1 + \frac{1}{2}\frac{4\pi e^2}{m_{\rm e}}\frac{1}{\omega^2}\frac{1}{H}\left[\bar{N}_{\rm e}^{(H)} + \left(\bar{N}_{\rm e}^{(H)} - N_{\rm e}(H)H\right)\left(\tan^2\theta_0 - \tan\theta_0\right)\right]\right\}, \tag{2.25}$$

where $\bar{N}_{\rm e}^{(H)}$ is the integral of the electron number density across the layer of thickness H; see formula (D.3).

Let us first notice that if the electron number density is constant, $N_{\rm e}(h) \equiv N_{\rm e}$, then, clearly, $\bar{N}_{\rm e}^{(H)} = N_{\rm e}H$, and formula (2.25) yields

$$T = \frac{R_{\boldsymbol{z}}}{c} + \frac{R_{\boldsymbol{z}}}{c}\frac{1}{2}\frac{4\pi e^2}{m_{\rm e}}\frac{N_{\rm e}}{\omega^2} = \frac{R_{\boldsymbol{z}}}{c}\left(1 + \frac{1}{2}\frac{\omega_{\rm pe}^2}{\omega^2}\right) \approx \frac{R_{\boldsymbol{z}}}{v_{\rm gr}}.$$

Otherwise, expression (2.25) for the travel time T, evaluated at the center carrier frequency ω_0 of the pulse as $T = T(\boldsymbol{x}, \boldsymbol{z}, \omega_0)$, shall be substituted instead of $R_{\boldsymbol{z}}/v_0$ into formula (2.14) and into all subsequent formulae of section 2.1.1. Similar expressions can be obtained for the travel times that correspond to the highest and lowest frequencies $\omega_{\max}$ and $\omega_{\min}$; see formula (2.10). Then, instead of (2.12) we will have

$$\delta\tau \approx \frac{2R_{\boldsymbol{z}}}{c}\frac{4\pi e^2}{m_{\rm e}\omega_0^2}\frac{\bar{N}}{H}\frac{B}{\omega_0}, \tag{2.26}$$

where

$$\bar{N} \stackrel{\rm def}{=} \left[\bar{N}_{\rm e}^{(H)} + \left(\bar{N}_{\rm e}^{(H)} - N_{\rm e}(H)H\right)\left(\tan^2\theta_0 - \tan\theta_0\right)\right] \tag{2.27}$$

is the quantity that characterizes the plasma; see formula (2.25). Similarly to section 2.1.1 (see formulae (2.18) and (C.5)), we will obtain a certain deterioration of the range resolution. It will not be large, though, because for the typical values of the parameters, the quantity $\delta\tau$ given by (2.26) is small (recall that in section 2.1.1 the quantity $\delta\tau$ of (2.12) was small). Indeed, for simplicity let us take $\theta_0 = 45^\circ$; then formula (2.27) yields $\bar{N} = \bar{N}_{\rm e}^{(H)}$, and the latter quantity is often estimated as $3\cdot 10^{13} cm^{-2}$ (see [2]).[3] As such, for $H = 500km$ the value $\bar{N}/H = 6\cdot 10^5 cm^{-3}$ that appears in formula (2.26) is even smaller than $\langle N_{\rm e}\rangle = 10^6 cm^{-3}$ that we used to estimate the Langmuir frequency for formula (2.12). Hence, we conclude that, as in section 2.1.1, the direct effect of the pulse dilation on the range resolution will be very small, $\sim 0.01\%$, whereas the deterioration of the image sharpness (contrast) due to smearing out of the extrema of the generalized ambiguity function can reach 1%. Of course, the quality of the image will improve if the carrier frequency ω_0 increases, and will deteriorate further if it decreases.

Besides, there will be a shift in the actual range of the target. This shift can also be removed by probing the ionosphere on two different frequencies, as in section 2.1.2. Indeed, the entire quantity $\bar{N}$ of (2.27) can be interpreted as one unknown. The second unknown is the range $R_{\boldsymbol{z}}$ from the antenna to the target. By probing on two frequencies and measuring the reference ranges $R_{\boldsymbol{y}}$ and $R_{\boldsymbol{y}}^{(1)}$, we will obtain a system of equations that can be solved for both the unknown range $R_{\boldsymbol{z}}$ and the plasma quantity $\bar{N}$; see section 3.

[3] More precisely, for sufficiently high orbit altitudes integration (D.3) can be replaced by integration across the entire ionosphere, and the resulting quantity $\bar{N}_{\rm e}^{(\infty)}$ is typically between $7.5\cdot 10^{12} cm^{-2}$ and $8\cdot 10^{13} cm^{-2}$, with the average being $3\cdot 10^{13} cm^{-2}$.

2.1.4. The effect of randomness. Up to this point, we have treated the electron number density $N_e = N_e(h)$ as a deterministic quantity. According to formula (1.7), however, the density has a random content, and we would like to see how it may affect the analysis and conclusions of sections 2.1.1–2.1.3.

The mean characteristics of the ionospheric plasma depend on the altitude, but do not depend on the horizontal coordinate(s). Hence, formula (1.7) becomes

$$N_e = \langle N_e(h) \rangle + \mu(\boldsymbol{x}), \tag{2.28}$$

where the fluctuating part of the density, $\mu(\boldsymbol{x})$, which is due to the turbulence, still depends on all spatial coordinates. Furthermore, the ionospheric quantities may vary not only in space but also in time. However, a typical time scale for the turbulent motions of the ionosphere is much slower than the time it takes for electromagnetic waves to propagate back and forth between the satellite and the ground (the latter is on the order of milliseconds). Hence, for the purpose of studying how the turbulent fluctuations may affect the electromagnetic propagation, we can freeze the time, i.e., consider a "snapshot" of the ionosphere.

Altogether, the quantity $\mu(\boldsymbol{x})$ of (2.28) is a quasi-homogeneous isotropic random field with zero mean. This implies that the correlation function defined by formula (1.8) depends on two variables, the "local" variable r and the altitude h: $V = V(r, h)$. The dependence on h is slow, and the dependence on r is fast, so that the spectrum of turbulence given by formula (1.9) can be redefined as the Fourier transform in the fast variable r only, and should be interpreted as a local spectrum [36, Chapter I].

The signals traveling through any particular realization of the field (2.28) undergo multiple scattering. This affects their characteristics, in particular, the travel times between the antenna and the target, that are of foremost importance for SAR applications. As we will see, however, the overall effect of randomness will be stronger for the cross-range (azimuthal) resolution (section 2.2) and weaker for the range resolution.

To study the effect of randomness on the resolution of a SAR sensor, we employ the geometrical optics perturbations method. It was developed in [37, Chapter 1] to compute statistics of the eikonal, travel times, and other quantities that characterize the waves propagating in random media. The advantage of this method is that it is relatively simple and allows one to analyze not only homogeneous random fields but also quasi-homogeneous fields, which is more difficult to do, say, when using the paraxial approximation [37]. For the geometrical optics approach to be valid (in this section, as well as in section 2.2.2 where we analyze azimuthal resolution), the wavelength λ must be much shorter than the characteristic scale of turbulent inhomogeneities. If the latter is taken as r_0 (the outer scale of turbulence), the constraint $\lambda \ll r_0$ is obviously met. It will still be met even for shorter scales, such as the inner scale of turbulence. There is, however, a more subtle criterion of applicability of the geometrical optics. The characteristic scale of inhomogeneities must be much longer than the size of the first Fresnel zone $\sqrt{\lambda R_z}$. The latter comes to approximately $540m$ for $\lambda = 30cm$ and $R_z = 1000km$, which is roughly $\frac{1}{2}r_0$ according to [2] or $\frac{1}{20}r_0$ according to [9], and is longer than the inner scale of turbulence. Technically speaking, this makes the geometrical optics a borderline approximation for the class of problems we are considering. It is known, however, that there are fewer shorter scale inhomogeneities in the spectrum of the ionospheric turbu-

lence than longer scale inhomogeneities, which still leaves the main conclusions of geometrical optics valid even outside its formal applicability range; see [37, Chapter I].

The key quantity that we want to obtain is the travel time for the signal propagating from the antenna to the target and back. To estimate it, we will assume that the trajectory of the signal is still the same as we obtained previously[4] (see Figure 1(b)), whereas the signal traveling along this trajectory crosses through the random inhomogeneities given by formula (2.28). This is precisely the first order perturbations approach, and all we need to do is take into account randomness (2.28) in the definition of the group velocity (D.6). At the same time, we do not need to introduce randomness into the definition of the trajectory (see formulae (2.22), (D.1), (D.5)); instead, we will keep $\omega_{\rm pe}^2(h) = \frac{4\pi e^2\langle N_{\rm e}(h)\rangle}{m_{\rm e}}$ in the corresponding expressions.

Let us begin with an even simpler case of the straight trajectory; see formula (2.24). Its total length is $R_{\boldsymbol{z}} = H/\cos\theta_0$ (see Figure 1(b)), and taking into account the variation of the group velocity we have

$$
\begin{aligned}
T &= \int_0^{R_z} \frac{dt}{ds} ds = \int_0^{R_z} \frac{1}{v_0} ds \approx \int_0^{R_z} \frac{1}{c}\left(1 + \frac{1}{2}\frac{\omega_{\rm pe}^2(h)}{\omega^2}\right) ds \\
&= \int_0^{H} \frac{1}{c}\left(1 + \frac{1}{2}\frac{4\pi e^2\langle N_{\rm e}(h)\rangle}{m_{\rm e}\omega^2}\right)\frac{dh}{\cos\theta_0} + \frac{1}{c}\int_0^{R_z}\frac{1}{2}\frac{4\pi e^2\mu(\boldsymbol{x})}{m_{\rm e}\omega^2} ds \\
&= \frac{R_{\boldsymbol{z}}}{c}\left\{1 + \frac{1}{2}\frac{4\pi e^2}{m_{\rm e}\omega^2}\frac{\bar{N}_{\rm e}^{(H)}}{H} + \frac{1}{2}\frac{4\pi e^2}{m_{\rm e}\omega^2}\cdot\frac{1}{R_{\boldsymbol{z}}}\int_0^{R_z}\mu(\boldsymbol{x})ds\right\}.
\end{aligned}
\tag{2.29}
$$

The first two terms in the brackets on the right-hand side of (2.29) will coincide with the corresponding terms on the right-hand side of (2.25) if we redefine the integral number density $\bar{N}_{\rm e}^{(H)}$ as follows:

$$
\bar{N}_{\rm e}^{(H)} \stackrel{\rm def}{=} \int_0^H \langle N_{\rm e}(h)\rangle dh. \tag{2.30}
$$

The remaining integral on the right-hand side of (2.29) is precisely what accounts for randomness of the medium. This integral is one-dimensional, and, consequently, we can interpret the quantity μ under the integral as a homogeneous random field on the line: $\mu = \mu(s)$. In turn, the one-dimensional interpretation enables a straightforward application of the ergodic theorem. The argument based on ergodicity is presented in Appendix E. It essentially implies that the statistical mean of μ can be substituted instead of its spatial average as needed. Since $\langle\mu\rangle = 0$, we expect that the contribution of the last integral on the right-hand side of (2.29) to the overall travel time is small, provided that the integration distance $R_{\boldsymbol{z}}$ is sufficiently large.

To actually quantify the effect of randomness on the resolution of a SAR sensor and compare it with that of the "baseline" dispersion due to $\langle N_{\rm e}(h)\rangle$, let us introduce

$$
\varphi \stackrel{\rm def}{=} \frac{4\pi e^2}{m_{\rm e}\omega^2}\int_0^{R_z}\mu(\boldsymbol{x})ds, \quad \text{where} \quad R_{\boldsymbol{z}} = |\boldsymbol{z} - \boldsymbol{x}^n|. \tag{2.31}
$$

[4]The only difference is that in this case, the mean electron number density $\langle N_{\rm e}(h)\rangle$ shall be substituted instead of the deterministic density $N_{\rm e}(h)$ into the corresponding expressions of section 2.1.3 and Appendix D.

The quantity φ has the dimension of length and can be interpreted as the first order perturbation of the eikonal, i.e., the phase path of the waves (see [37, Chapter I]), due to turbulent fluctuations of the electron number density. Then, we use formulae (2.29), (2.31) to evaluate the travel times for the maximum and minimum frequencies $\omega_{\max} = \omega_0 + B/2$ and $\omega_{\min} = \omega_0 - B/2$ (see formula (2.2)), and compute the temporal dilation of the pulse $\delta\tau$ yet one more time (cf. formulae (2.12) and (2.26)), now with random contribution included:

$$\delta\tau \approx \frac{2R_z}{c}\frac{4\pi e^2}{m_e\omega_0^2}\frac{\bar{N}_e^{(H)}}{H}\frac{B}{\omega_0} + \frac{2R_z}{c}\frac{\varphi}{R_z}\frac{B}{\omega_0}. \tag{2.32}$$

Next, as $\langle\mu\rangle = 0$, we also have $\langle\varphi\rangle = 0$. Moreover, it is shown in [37, Chapter I] that in the simplest case of a homogeneous medium

$$\langle\varphi^2\rangle = \left(\frac{4\pi e^2}{m_e\omega^2}\right)^2 \pi^2 R_z \int_0^\infty \hat{V}(q) q dq,$$

where $\hat{V}(q)$ is the spectrum of fluctuations. Using formula (1.10) with $\kappa = 2$ and formula (1.13), we have

$$\langle\varphi^2\rangle = \left(\frac{4\pi e^2}{m_e\omega^2}\right)^2 \pi^2 R_z \frac{Cq_0^2}{2(\kappa-1)} = \left(\frac{4\pi e^2}{m_e\omega^2}\right) R_z^2 \frac{\langle\mu^2\rangle}{q_0} = \left(\frac{4\pi e^2}{m_e\omega^2}\right)^2 R_z r_0 \langle\mu^2\rangle, \tag{2.33}$$

where $\langle\mu^2\rangle = \text{const}$ in the homogeneous case. Consequently, formula (2.32) along with (2.33) yields

$$\langle\delta\tau\rangle = \frac{2R_z}{c}\frac{4\pi e^2}{m_e\omega_0^2}\frac{\bar{N}_e^{(H)}}{H}\frac{B}{\omega_0} \quad \text{and} \quad \sqrt{\langle\delta\tau^2\rangle} = \frac{2R_z}{c}\frac{4\pi e^2}{m_e\omega_0^2}\sqrt{\frac{r_0}{R_z}}\sqrt{\langle\mu^2\rangle}\frac{B}{\omega_0}. \tag{2.34}$$

The first quantity in formula (2.34), $\langle\delta\tau\rangle$, is the mean temporal dilation of the pulse, which coincides with the deterministic value (2.26). The random contribution to the dilation is natural to estimate by the standard deviation $\sqrt{\langle\delta\tau^2\rangle}$. Hence, we need to compare two quantities: $\frac{4\pi e^2}{m_e\omega_0^2}\frac{\bar{N}_e^{(H)}}{H}$ and $\sqrt{\frac{r_0}{R_z}}\frac{4\pi e^2}{m_e\omega_0^2}\sqrt{\langle\mu^2\rangle}$. As we saw in section 2.1.3, the value of $\bar{N}_e^{(H)}/H$ is close to $\langle N_e\rangle$ when the latter is interpreted as a constant, $\langle N_e\rangle \sim 10^6 cm^{-3}$. At the same time, the ratio $M = \sqrt{\langle\mu^2\rangle}/\langle N_e\rangle$ (see formula (1.14)) does not exceed 10^{-1} and typically is much smaller. Besides, the factor $\sqrt{\frac{r_0}{R_z}}$ is also small. Altogether, we conclude that the contribution of turbulent fluctuations (of the electron number density) to the temporal dilation of the radar pulse is smaller by a factor of $\sqrt{\frac{r_0}{R_z}}\frac{\sqrt{\langle\mu^2\rangle}}{\langle N_e\rangle} \ll 1$ than the original dilation due to the baseline dispersion. The latter is small in its own right (sections 2.1.1 and 2.1.3) and, according to formulae (2.18), (2.13), and (C.5), may cause only a small deterioration of the image quality in range. More precisely, there may be about 1% degradation of the contrast. Hence, the role of randomness is much smaller than 1%.

In the full inhomogeneous case (stratified ionosphere with variable mean density $\langle N_e(h)\rangle$), two modifications of the previous analysis need to be implemented. Besides accounting for the variation of the group velocity with altitude by formula (2.29), we need to take into account

that the variance of fluctuations becomes altitude dependent as well, $\langle\mu^2\rangle = \langle\mu^2(h)\rangle$, and also that the ray trajectory between the antenna and the target becomes bent. First, expression (2.33) is to be replaced by [37, Chapter I]

$$\langle\varphi^2\rangle = r_0 \int_0^{R_z} \frac{\left(\frac{4\pi e^2}{m_e\omega_0^2}\right)^2 \langle\mu^2(s)\rangle}{1 - \frac{4\pi e^2\langle N_e(s)\rangle}{m_e\omega_0^2}} ds \approx \frac{r_0}{\cos\theta_0}\left(\frac{4\pi e^2}{m_e\omega_0^2}\right)^2 \int_0^H \langle\mu^2(h)\rangle dh, \tag{2.35}$$

where the numerator under the first integral is the variance of the fluctuating part of the electric permittivity and the denominator is the mean electric permittivity. The latter is subsequently replaced by 1 in the context of linearization, because $\frac{4\pi e^2\langle N_e(s)\rangle}{m_e\omega_0^2} \ll 1$. Next, as the ratio M given by (1.14) does not depend on the altitude, we can write instead of (2.35)

$$\langle\varphi^2\rangle = \frac{r_0}{\cos\theta_0}\left(\frac{4\pi e^2}{m_e\omega_0^2}\right)^2 M^2 \int_0^H \langle N_e(h)\rangle^2 dh \stackrel{\text{def}}{=} \frac{r_0}{\cos\theta_0}\left(\frac{4\pi e^2}{m_e\omega_0^2}\right)^2 M^2 \bar{N}_e^{2,(H)}. \tag{2.36}$$

According to [2], the value of $\bar{N}_e^{2,(H)}$ (rather, $\bar{N}_e^{2,(\infty)}$, which is the same for high altitudes H) is between $9.3\cdot 10^{18} cm^{-5}$ and $9.9\cdot 10^{20} cm^{-5}$, with the average about $1.5\cdot 10^{19} cm^{-5}$. Then, for $r_0 = 10^5 cm$, $M = 5\cdot 10^{-3}$, and $\theta_0 = 45^\circ$, formula (2.36) yields $\langle\varphi^2\rangle \approx 3.4 cm^2$. This value is close to $\langle\varphi^2\rangle = (\frac{\omega_{pe}^2}{\omega_0^2})^2 M^2 R_z r_0 \approx 2.5 cm^2$, given by formula (2.33) for $R_z = 1000 km$ and $\frac{\omega_{pe}^2}{\omega_0^2} = 10^{-4}$. Hence, the previous determination that the effect of randomness on the range resolution is small is still valid.

Finally, we need to integrate along the actual trajectory shown in Figure 1(b) rather than along the straight line (2.24). We will not conduct the analysis here, but will present only an intuitive argument. Since the ionospheric corrections are generally small for high carrier frequencies, $\omega_0 \gg \omega_{pe}$, and the characteristic scale of variations for $\langle N_e(h)\rangle$ is much larger than r_0, the actual trajectory is close to the straight line (2.24), and its radius of curvature is large (much larger than the correlation length r_0). Then, the field $\mu(\boldsymbol{x})$ considered along the trajectory can also be interpreted as a one-dimensional homogeneous random field $\mu = \mu(s)$, where s is the arc length. Hence, the previous argument will extend to this case with no change. Note that the possibility of integrating along the slightly bent deterministic rays is also mentioned in [37].

To summarize, if the fluctuations of the electron number density are small, then we can use linearization (see [37, Chapter 1]), in order to evaluate the wave arrival times in the presence of randomness. The linearization implies that randomness of the ionosphere may affect only the group speed along the wave trajectory, while the trajectory itself remains deterministic.[5] Then, the effect of randomness on the range resolution of a spaceborne SAR sensor appears much smaller than that of the baseline dispersion.

[5]Indeed, if the effect of randomness on the shape of the trajectory is taken into account (see, e.g., [37, section 2]), then the corresponding ray shift will be small and the resulting effect on the arrival time will be a second order perturbation.

2.2. Azimuthal resolution. The azimuthal part of the generalized ambiguity function is given by formula (2.8), where $\boldsymbol{z}$ is the location of the target, $\boldsymbol{y}$ is the location of the reference point (they are now at the same range R_0), and $\boldsymbol{x}^n$ is the location of the antenna at the moment it emits the nth pulse.

2.2.1. Ionospheric corrections. To take into account the ionosphere, we need to replace $\frac{|\boldsymbol{z}-\boldsymbol{x}^n|}{c}$ in formula (2.8) by the actual travel time between the antenna and the target. Disregarding the ionospheric fluctuations for the moment, we can take the travel time in the form suggested by (2.25):

$$T(\boldsymbol{z},\boldsymbol{x}^n)=\frac{|\boldsymbol{z}-\boldsymbol{x}^n|}{c}\left[1+\frac{1}{2}\frac{4\pi e^2}{m_{\rm e}}\frac{1}{\omega^2}\frac{\bar N_{\rm e}^{(H)}}{H}\right], \tag{2.37}$$

where we have dropped the term $\sim(\tan^2\theta_0-\tan\theta_0)$ for simplicity, say, because we can take $\theta_0=\pi/4$. We emphasize that the latter simplification is aimed only at making the subsequent derivations less cumbersome. Other than that, it does not lead to a qualitative change in the conclusions, and if a good estimate is available for the quantity $N_{\rm e}(H)$ (see formula (2.25)), then the term $\sim(\tan^2\theta_0-\tan\theta_0)$ can be brought back. For the typical values of the parameters introduced earlier, $\omega=1GHz$, $\bar N_{\rm e}^{(H)}=3\cdot10^{13}cm^{-2}$, and $H=500km$, the magnitude of the correction term, i.e., the second term in the brackets in formula (2.37), is $\sim 2.42\cdot10^{-5}$.

For the travel distances that appear in formulae (2.8) and (2.37) we can write [11]

$$\begin{aligned}
R_{\boldsymbol{z}}&=|\boldsymbol{z}-\boldsymbol{x}^n|=\sqrt{R_0^2+(z_1-x_1^n)^2}=R_0\sqrt{1+\frac{(x_1^n)^2}{R_0^2}}\approx R_0\left(1+\frac{1}{2}\frac{(x_1^n)^2}{R_0^2}\right),\\
R_{\boldsymbol{y}}&=|\boldsymbol{y}-\boldsymbol{x}^n|=\sqrt{R_0^2+(y_1-x_1^n)^2}=R_0\sqrt{1+\frac{(y_1-x_1^n)^2}{R_0^2}}\approx R_0\left(1+\frac{1}{2}\frac{(y_1-x_1^n)^2}{R_0^2}\right),
\end{aligned} \tag{2.38}$$

where we have made a natural assumption that $|x_1^n|\ll R_0$ and $|y_1-x_1^n|\ll R_0$ (recall that the subscript "1" denotes the coordinate along the orbit, and $z_1=0$). Substituting these expressions into (2.8), we obtain

$$\begin{aligned}
W_A(\boldsymbol{y},\boldsymbol{z})&\approx\sum_{n=-N/2}^{N/2}e^{2i\omega_0\left(\left(R_0+\frac12\frac{(y_1-x_1^n)^2}{R_0}\right)\frac1c-\left(R_0+\frac12\frac{(x_1^n)^2}{R_0}\right)\frac1c\left[1+\frac12\frac{4\pi e^2}{m_{\rm e}}\frac{1}{\omega_0^2}\frac{\bar N_{\rm e}^{(H)}}{H}\right]\right)}\\
&=e^{2i\omega_0\left(\frac12\frac{y_1^2}{R_0c}-\frac{R_0}{c}\frac12\frac{4\pi e^2}{m_{\rm e}}\frac{1}{\omega_0^2}\frac{\bar N_{\rm e}^{(H)}}{H}\right)}\sum_{n=-N/2}^{N/2}e^{2i\omega_0\left(-\frac{y_1x_1^n}{R_0c}-\frac12\frac{(x_1^n)^2}{R_0c}\frac12\frac{4\pi e^2}{m_{\rm e}}\frac{1}{\omega_0^2}\frac{\bar N_{\rm e}^{(H)}}{H}\right)},
\end{aligned} \tag{2.39}$$

where we have evaluated the travel time (2.37) at the center carrier frequency ω_0, and all the factors independent of the summation index n have been taken outside of the sum in (2.39).

Next, to actually compute the sum on the right-hand side of (2.39) we will approximate it by an integral. Recall that $x_1^n=n\cdot\Delta x_1$, and denote

$$a=\frac{2\omega_0y_1\Delta x_1}{R_0c}\quad\text{and}\quad b=\frac{\omega_0(\Delta x_1)^2}{2R_0c}\frac{4\pi e^2}{m_{\rm e}}\frac{\bar N_{\rm e}^{(H)}}{\omega_0^2H}.$$

Then, we can write

$$\sum_{n=-N/2}^{N/2} e^{-ian-ibn^2} \approx \int_{-(N+1)/2}^{(N+1)/2} e^{-iau-ibu^2} du. \tag{2.40}$$

Formula (2.40) can be interpreted as a conventional midpoint quadrature rule for the integral on its right-hand side. Its absolute error is bounded by the maximum absolute value of the second derivative of the integrand, times the square of the grid size (equal to 1), and times the length of the integration interval (which is $N+1$); see, e.g., [35, section 4.1]. To estimate the relative error, we temporarily disregard the ionospheric correction (i.e., take $b=0$) and evaluate

$$\max_a \left| \int_{-(N+1)/2}^{(N+1)/2} e^{-iau} du \right| = \max_a \left| \frac{2\sin\frac{a(N+1)}{2}}{a} \right| = N+1,$$

which indicates that the relative error of formula (2.40) is $\mathcal{O}(a^2)$. Hence, approximation (2.40) can only be used for small values of y_1:

$$a \ll 1 \implies y_1 \ll \frac{R_0 c}{2\omega_0 \Delta x_1} = \frac{\lambda R_0}{4\pi \Delta x_1}. \tag{2.41}$$

Note that the two assumptions made when deriving formulae (2.38), namely, $|x_1^n| \ll R_0$ and $|y_1 - x_1^n| \ll R_0$, imply that both the target at $z_1 = 0$ and the reference location y_1 must be close to the center of the antenna footprint on the ground x_1^n. Hence, the left-hand side of the second inequality in (2.41) is not changing arbitrarily depending on where we image. This inequality should rather be interpreted as the requirement that the distance between the reference location y_1 and the target $z_1 = 0$ be small. Specifically, if $\lambda = 30cm$ ($\omega_0 = 1GHz$), $R_0 = 1000km$, and $\Delta x_1 = 4 \cdot 10^2 cm$, which is typical, then the value of the right-hand side of (2.41) is $\sim 6 \cdot 10^5 cm$. We will see, however, that this constraint presents no limitation for the resolution analysis, because the resulting azimuthal resolution will appear much shorter than the bound given by (2.41). We also note that the integral approximation (2.40) is needed only to take care of the quadratic term in the exponent. With no quadratic term, $b=0$; i.e., with no ionospheric correction, the sum of the exponentials can be computed directly (see [11]) as

$$\sum_{n=-N/2}^{N/2} e^{-ian} = \sum_{n=-N/2}^{N/2} (e^{-ia})^n = e^{i\frac{aN}{2}} \sum_{n=0}^{N} (e^{-ia})^n = e^{i\frac{aN}{2}} \frac{1-e^{-ia(N+1)}}{1-e^{-ia}} = \frac{\sin\frac{a(N+1)}{2}}{\sin\frac{a}{2}},$$

and for $a \ll 1$ (which means, in particular, that inequality (2.41) must still hold) we have

$$\sum_{n=-N/2}^{N/2} e^{-ian} \approx (N+1)\mathrm{sinc}\frac{a(N+1)}{2}.$$

From $W_A(\boldsymbol{y}, \boldsymbol{z}) \propto \mathrm{sinc}\frac{a(N+1)}{2}$, the azimuthal resolution is obtained as the width of the sinc function:

$$a = \frac{2\pi}{N+1} \implies y_1 \frac{4\pi\Delta x_1}{\lambda R_0} \approx \frac{\pi \Delta x_1 L}{\lambda R_0} \implies 2y_1 \approx \frac{L}{2}, \tag{2.42}$$

where L is the antenna size. Formula (2.42) yields the minimum cross-range distance $2y_1$ between the reference point $\boldsymbol{y}$ and the target at $\boldsymbol{z} = \boldsymbol{0}$ that the SAR sensor can resolve in the absence of distortions.

To address the ionospheric distortions (with no fluctuations yet), we return to the integral (2.40):

$$
\begin{aligned}
W_A(\boldsymbol{y},\boldsymbol{z}) &\propto \int_{-(N+1)/2}^{(N+1)/2} e^{-iau-ibu^2}\,du \\
&= \frac{\sqrt{\pi}}{2\sqrt{b}} e^{i\frac{a^2}{4b}-i\frac{\pi}{4}} \left(\operatorname{erf}\left[\frac{\sqrt{i}(a+b(N+1))}{2\sqrt{b}}\right] - \operatorname{erf}\left[\frac{\sqrt{i}(a-b(N+1))}{2\sqrt{b}}\right]\right).
\end{aligned} \tag{2.43}
$$

Comparing formula (2.43) with formula (C.4), we conclude that they are virtually identical, the only difference being in the signs and in the notation for the parameters. Consequently, the same conclusions as those we reached at the end of section 2.1.1 regarding the function $|W_R'(\boldsymbol{y},\boldsymbol{z})|$ will apply to the function $|W_A(\boldsymbol{y},\boldsymbol{z})|$.

Specifically, the width of the main lobe of $|W_A(\boldsymbol{y},\boldsymbol{z})|$ is the same as that of $\operatorname{sinc}\frac{a(N+1)}{2}$, provided that the former is redefined as twice the distance between the central maximum of the function and its first minimum. Therefore, if the azimuthal resolution of a SAR sensor is judged only by the width of the main lobe of the ambiguity function, then it basically remains unaffected by the nonfluctuating ionosphere. However, the second consideration outlined at the end of section 2.1.1, namely, the "sharpness" of the minimum, may become even more important as it applies to $W_A(\boldsymbol{y},\boldsymbol{z})$ of (2.43).

Similarly to (C.5), we can write

$$
|W_A(\boldsymbol{y},\boldsymbol{z})|\Big|_{a=\frac{2\pi}{N+1}} = (N+1)\cdot\frac{b(N+1)^2}{2\pi^2}\cdot\left(1-\frac{i(\pi^2-6)b(N+1)^2}{4\pi^2}+\mathcal{O}\left(b^2(N+1)^4\right)\right), \tag{2.44a}
$$

which for the typical values of the parameters chosen previously yields

$$
|W_A(\boldsymbol{y},\boldsymbol{z})|\Big|_{a=\frac{2\pi}{N+1}} \approx (N+1)\cdot 0.09. \tag{2.44b}
$$

Hence, the minimum (2.44a)–(2.44b) appears not nearly as sharp as the minimum (C.5), with the value of the former being about 9% of the central maximum. This is a substantial deterioration of contrast.

2.2.2. The effect of randomness. To take into account randomness in the context of azimuthal resolution, we need to replace the deterministic travel times (2.37) by the stochastic times (2.29) in the exponents in formula (2.39). Then, we will need to compute the expected

value and the variance of the resulting sum. To begin with, we write instead of (2.39)

(2.45)
$$W_A(\boldsymbol{y},\boldsymbol{z}) \approx e^{2i\omega_0\left(\frac{y_1^2}{2R_0c}-\frac{R_0}{2c}\frac{4\pi e^2}{m_e\omega_0^2}\frac{\bar{N}_e^{(H)}}{H}\right)} \sum_{n=-N/2}^{N/2} e^{\frac{2i\omega_0}{c}\left(-\frac{y_1x_1^n}{R_0}-\frac{(x_1^n)^2}{2R_0}\frac{4\pi e^2}{m_e\omega_0^2}\frac{\bar{N}_e^{(H)}}{2H}-\frac{1}{2}\frac{4\pi e^2}{m_e\omega_0^2}\int_0^{R_z}\mu(\boldsymbol{x})ds\right)}$$
$$= e^{2i\omega_0\left(\frac{y_1^2}{2R_0c}-\frac{R_0}{2c}\frac{4\pi e^2}{m_e\omega_0^2}\frac{\bar{N}_e^{(H)}}{H}\right)} \sum_{n=-N/2}^{N/2} e^{-ian-ibn^2-\frac{i\omega_0}{c}\varphi_n}.$$

The random contribution to the eikonal in each term on the right-hand side of (2.45) is $\varphi_n = \varphi(\boldsymbol{x}^n,\boldsymbol{z})$ given by formula (2.31). Our subsequent analysis will rely on the following proposition [37, Chapter I].

Proposition 2.1. *For sufficiently large integration distances $R_{\boldsymbol{z}}$, each quantity φ_n becomes a Gaussian random variable with zero mean. This is an implication of* the central limit theorem *(see, e.g., [14]), because the integration path crosses through many identically distributed inhomogeneities.*

An important comment is in order regarding the correct interpretation of Proposition 2.1. If the integral on the right-hand side of formula (2.31) was normalized by $1/\sqrt{R_{\boldsymbol{z}}}$, then a straightforward application of the central limit theorem would imply weak convergence to the Gaussian probability distribution function with zero mean and the variance equal to 1. We, however, consider the actual nonnormalized perturbation of the eikonal φ. It still has zero mean, but its variance grows linearly (in the homogeneous case) as the integration distance $R_{\boldsymbol{z}}$ increases; see formula (2.33). Consequently, the resulting Gaussian will also have a growing variance. This interpretation is encountered frequently; see [37, Chapter I] and also [38].

For any fixed n, Proposition 2.1 yields

(2.46)
$$\langle e^{-ian-ibn^2-\frac{i\omega_0}{c}\varphi_n}\rangle = e^{-ian-ibn^2}\frac{1}{\sqrt{2\pi\langle\varphi_n^2\rangle}}\int_{-\infty}^{\infty} e^{-\frac{i\omega_0}{c}\xi}e^{\frac{-\xi^2}{2\langle\varphi_n^2\rangle}}d\xi = e^{-ian-ibn^2}e^{-\frac{1}{2}\frac{\omega_0^2}{c^2}\langle\varphi_n^2\rangle}.$$

We first observe a decrease in the amplitude of the mean value of each term in the sum due to multiple scattering. In the literature, this phenomenon is sometimes is referred to as "extinction"; see [37, Chapter I]. For the typical values of parameters, including M of (1.14) taken as $M = \sqrt{\langle\mu^2\rangle}/\langle N_e\rangle = 5\cdot 10^{-3}$, we can estimate the value of the last exponent in formula (2.46) with the help of formula (2.36), which yields $\frac{1}{2}\frac{\omega_0^2}{c^2}\langle\varphi_n^2\rangle \approx 1.88\cdot 10^{-3}$. Hence, the extinction is small and will further decrease inversely proportional to the square of the carrier frequency, $\sim\omega_0^{-2}$, as the latter increases.

Next, we compute the variance of each term (a complex random variable) in the sum (2.45):

(2.47a)
$$\sigma_n^2 = \langle|e^{-ian-ibn^2-\frac{i\omega_0}{c}\varphi_n} - e^{-ian-ibn^2}e^{-\frac{1}{2}\frac{\omega_0^2}{c^2}\langle\varphi_n^2\rangle}|^2\rangle = \langle|e^{-\frac{i\omega_0}{c}\varphi_n} - e^{-\frac{1}{2}\frac{\omega_0^2}{c^2}\langle\varphi_n^2\rangle}|^2\rangle$$
$$= \frac{1}{\sqrt{2\pi\langle\varphi_n^2\rangle}}\int_{-\infty}^{\infty}\left|e^{-\frac{i\omega_0}{c}\xi} - e^{-\frac{1}{2}\frac{\omega_0^2}{c^2}\langle\varphi_n^2\rangle}\right|^2 e^{\frac{-\xi^2}{2\langle\varphi_n^2\rangle}}d\xi = e^{-\frac{\omega_0^2}{c^2}\langle\varphi_n^2\rangle}(e^{\frac{\omega_0^2}{c^2}\langle\varphi_n^2\rangle}-1).$$

Then, since the variance of the phase $\frac{\omega_0^2}{c^2}\langle\varphi_n^2\rangle$ is small, we use Taylor's expansion and obtain from (2.47a)

$$\sigma_n^2 \approx \frac{\omega_0^2}{c^2}\langle\varphi_n^2\rangle. \tag{2.47b}$$

Expression (2.47b) gives variances for the individual terms in the sum (2.45). Technically speaking, they are all different because $R_{\boldsymbol{z}}$ depends on n in formulae (2.31) and (2.33). However, for the purpose of approximately estimating how "bad" the randomness may be for azimuthal resolution, we will take

$$\sigma_n^2 \approx \sigma^2, \quad n = -N/2, \ldots, N/2, \tag{2.48}$$

because the variation of $R_{\boldsymbol{z}}$ as a function of n is small. To obtain the variance of the entire sum, we need to make an assumption regarding the dependence or independence of its individual terms. We will first consider the best case scenario and the worst case scenario, and thus derive a lower bound and an upper bound.

Assume that all the terms in the sum (2.45) are independent. Then, for its variance we can write

$$\sigma_\Sigma^2 = (N+1)\sigma^2. \tag{2.49}$$

Hence, one can think that the actual value of the sum for a particular realization of $\mu(\boldsymbol{x})$ may be anywhere within the σ_Σ range from the deterministic value given by formulae (2.39), (2.40), and (2.43).[6] In section 2.2.1, we have shown that the deterministic ionospheric distortions do not change the width of the main lobe of the ambiguity function but rather reduce the sharpness of its maxima and minima. In contrast, random contributions can obviously shift the locations of those extrema. The simplest estimate can be obtained as follows. Take the undistorted ambiguity function $W = (N+1)\mathrm{sinc}\frac{a(N+1)}{2} = \frac{\sin a(N+1)/2}{a/2}$ that has its first zero at $a = 2\pi/(N+1)$. For this function, we have

$$\left.\frac{dW}{da}\right|_{a=\frac{2\pi}{N+1}} = -\frac{(N+1)^2}{\pi}.$$

Then, given that the value of the function may change by σ_Σ, the location of the zero may shift by

$$\sigma_\Sigma \cdot \left| \left(\left.\frac{dW}{da}\right|_{a=\frac{2\pi}{N+1}} \right)^{-1} \right| = \frac{\pi\sigma}{(N+1)^{3/2}} = \frac{2\pi}{N+1} \cdot \frac{\sigma}{2(N+1)^{1/2}}.$$

Hence, the relative change in the resolution can be estimated as $\sigma/2\sqrt{N+1}$, which is about 0.022% for the typical values of the parameters that we have used. This change is still quite small. It can, however, be considered only a lower bound because all the terms in the

[6] We disregard the extinction (2.46) when evaluating the mean of the sum (2.45) and take it as merely the deterministic value. However, extinction is obviously taken into account when computing the individual variances (2.47a).

sum (2.45) cannot be independent random variables. Indeed, for two successive transmitting positions of the antenna the ray trajectories will be crossing through practically the same fluctuations. On the other hand, in the worst case scenario all the random variables in the sum (2.45) are to be assumed identical, which yields

$$\sigma_\Sigma^2 = (N+1)^2\sigma^2. \tag{2.50}$$

Then the relative change in the resolution will be $\sigma/2$ rather than $\sigma/2\sqrt{N+1}$, which is about 2.2% for our typical set of parameters, and which is already noticeable.

To get a better understanding of the dependence or independence of individual random variables in the sum (2.45) and to obtain a more accurate estimate of its variance, we first notice that since all the eikonals φ_n are normally distributed (according to Proposition 2.1), each term in the sum (2.45) has a logarithmically normal probability distribution. For regular Gaussian random variables it is known that if they are uncorrelated, then they are independent; see, e.g., [14, Chapter 2] or [22, Chapter 5]. *The same is, in fact, true for logarithmically normal random variables,* as shown in Appendix F. Therefore, if we were to obtain a correlation function (covariance) of the received field along the synthetic antenna (recall that each term in (2.45) represents the received field, up to a multiplicative factor), then it also would have provided a measure of dependence or independence for the random variables that compose the sum (2.45).

The required correlation function for the field has, in fact, been constructed in [37, Chapter I]; it is closely related to the so-called coherence function. Moreover, it is shown that if the fluctuations of the phase are small, then the correlation function for the field approximately coincides with the correlation function for the density (1.8). This is precisely the case for our analysis, because the variance of the phase $\frac{\omega_0^2}{c^2}\langle\varphi^2\rangle$ is indeed small. Consequently, the correlation length r_0 introduced by formula (1.12) for the turbulent fluctuations of the electron number density will also provide a characteristic scale of how rapidly the received field will decorrelate along the synthetic antenna. Roughly speaking, one can say that for the locations that are further apart than r_0 from one another, the received pulses will be uncorrelated and hence independent, whereas for the locations that are closer than r_0 to one another, they will not be independent.

Recall that the variances of the individual terms in the sum (2.45) are close to one another; see (2.48). Then, at the risk of somewhat simplifying the situation, we will artificially split the synthetic array into several clusters of elements with the length r_0, and assume that the random variables from the sum (2.45) that belong to a given cluster are identical, whereas for different clusters they are independent. The total length of the array can be estimated as

$$D = R_0\frac{2\lambda}{L},$$

where R_0 is the distance from the antenna to the target and $\frac{2\lambda}{L}$ is the angular beam width of the antenna. Therefore, the number of clusters is $\sim \frac{D}{r_0}$, and the number of elements in each cluster is

$$N_c \approx (N+1)\frac{r_0}{D} \approx \frac{r_0}{\Delta x_1}.$$

For the variance of the sum (2.45) we will therefore be getting the answer between the best case scenario (2.49) and the worst case scenario (2.50):

$$\sigma_\Sigma^2 = \frac{D}{r_0} N_c^2 \sigma^2 = \frac{r_0}{D}(N+1)^2\sigma^2. \tag{2.51}$$

This leads to the following expression for the relative change in the azimuthal resolution:

$$\frac{\sigma}{2}\sqrt{\frac{r_0}{D}}.$$

For the typical parameters we have chosen, the value of the square root in the previous formula is approximately 0.13, which yields about 0.3% deterioration in the azimuthal resolution.

It is also important to understand what will happen if the carrier frequency ω_0 changes. According to formulae (2.36), (2.47b), and (2.48), the standard deviation is inversely proportional to the carrier frequency:

$$\sigma \propto \omega_0^{-1}.$$

The same is true for the length of the array: $D \propto \omega_0^{-1}$. Hence, for the change in the resolution we have

$$\frac{\sigma}{2}\sqrt{\frac{r_0}{D}} \propto \frac{1}{\sqrt{\omega_0}}.$$

If, for example, we take the frequency in the VHF band, $\omega_0 = 300MHz$, which corresponds to the wavelength in vacuum $\lambda = 1m$, then the deterioration of the azimuthal resolution due to randomness will be about 0.5%.

The negative impact on the resolution that we have obtained, although not negligible, is still rather small. However, when estimating σ via $\langle\varphi^2\rangle$ (see formula (2.36)), we have taken the average values for M and $N_{\mathrm{e}}^{2,(H)}$. Taking the corresponding values from the upper part of their respective ranges (each of these two parameters can be at least an order of magnitude higher) will result in a much larger value of $\langle\varphi^2\rangle$ (about three orders of magnitude) and a most noticeable deterioration of the azimuthal resolution; see (2.51).

Let us finally note that the role of randomness in the deterioration of azimuthal resolution compared to the range resolution is relatively large. This can be qualitatively explained by "unaveraging." Namely, the range is measured by just the travel time, and the corresponding random contribution almost averages out due to ergodicity. However, in the case of azimuthal resolution many random variables are combined in the sum (2.45), and the effect of summation counterbalances the averaging.

3. Probing on two frequencies. In this section, we return to the idea of probing the scene and hence the ionosphere on two different carrier frequencies (first introduced in section 2.1.2), but exploit it in a somewhat more general perspective. Let us assume that there is an object or feature in the scene that can be clearly identified on the image. This object does not have to be artificial. It does not have to dominate the scene, say, by having the highest reflectivity. Its location does not have to be known ahead of time. It merely has to be something that can be fairly easily picked out and matched on different images. For example, it can be some landmark, a hilltop, a building, a road intersection, etc.

Let ω_0 and ω_1 be two distinct carrier frequencies, and let $R_{\boldsymbol{y}}^{(0)}$ and $R_{\boldsymbol{y}}^{(1)}$ be the corresponding ranges of the aforementioned object measured by the radar, whereas its true range is $R_{\boldsymbol{z}}$. Then, we can recast system (2.17), (2.20), taking into account the inhomogeneity of the ionosphere, as

$$\begin{aligned} R_{\boldsymbol{y}}^{(0)} &= cT(\boldsymbol{x}^n, \boldsymbol{z}, \omega_0), \\ R_{\boldsymbol{y}}^{(1)} &= cT(\boldsymbol{x}^n, \boldsymbol{z}, \omega_1), \end{aligned} \tag{3.1}$$

where the travel time T is determined according to formulae (2.25), (2.29):

$$\begin{aligned} T(\boldsymbol{x}^n, \boldsymbol{z}, \omega) &= \frac{R_{\boldsymbol{z}}}{c}\left\{1 + \frac{1}{2}\frac{4\pi e^2}{m_{\mathrm{e}}\omega^2}\frac{\bar{N}}{H} + \frac{1}{2}\frac{4\pi e^2}{m_{\mathrm{e}}\omega^2}\cdot\frac{1}{R_{\boldsymbol{z}}}\int_0^{R_z}\mu(\boldsymbol{x})ds\right\} \\ &= \frac{R_{\boldsymbol{z}}}{c}\left\{1 + \frac{1}{\omega^2}\frac{4\pi e^2}{2m_{\mathrm{e}}}\Bigg(\underbrace{\frac{\bar{N}}{H} + \frac{1}{R_{\boldsymbol{z}}}\int_0^{R_z}\mu(\boldsymbol{x})ds}_{\mathcal{N}}\Bigg)\right\}. \end{aligned} \tag{3.2}$$

The plasma quantity $\bar{N}$ that enters into (3.2) is given by formula (2.27). Note that formula (3.2) takes into account the contributions from both the mean electron number density $\langle N_{\mathrm{e}}(h)\rangle$ and its turbulent fluctuations—a particular realization of $\mu(\boldsymbol{x})$ at the time and place the images are taken.

With the data $R_{\boldsymbol{y}}^{(0)}$ and $R_{\boldsymbol{y}}^{(1)}$ available, system (3.1) can be solved with respect to the two unknown quantities: the true range $R_{\boldsymbol{z}}$ and the integral quantity $\mathcal{N}$ that characterizes the plasma; see formula (3.2). These two quantities can be used to modify the matched filter $P(t - t_n - 2|\boldsymbol{y} - \boldsymbol{x}^n|/c)$ in formula (2.3). Namely, the dilation of the pulse has to be taken into account in the filter (rather than only in the received signal) by first evaluating $\delta\tau$ according to (cf. formula (2.32))

$$\delta\tau \approx \frac{2R_{\boldsymbol{z}}}{c}\frac{4\pi e^2}{m_{\mathrm{e}}\omega_0^2}\frac{B}{\omega_0}\left(\frac{\bar{N}}{H} + \frac{1}{R_{\boldsymbol{z}}}\int_0^{R_z}\mu(\boldsymbol{x})ds\right) = \frac{2R_{\boldsymbol{z}}}{c}\frac{4\pi e^2}{m_{\mathrm{e}}\omega_0^2}\frac{B}{\omega_0}\mathcal{N}, \tag{3.3}$$

and then $\delta\alpha$ according to (2.13). Moreover, the round-trip travel time $2|\boldsymbol{y} - \boldsymbol{x}^n|/c$ has to be replaced by the expression similar to (3.2), but with the reference distance $R_{\boldsymbol{y}} = |\boldsymbol{y} - \boldsymbol{x}^n|$ substituted for $R_{\boldsymbol{z}}$ (except in $\mathcal{N}$):

$$2T(\boldsymbol{x}^n, \boldsymbol{y}, \omega) = \frac{2R_{\boldsymbol{y}}}{c} + \frac{R_{\boldsymbol{y}}}{c}\frac{1}{\omega^2}\frac{4\pi e^2}{m_{\mathrm{e}}}\left(\frac{\bar{N}}{H} + \frac{1}{R_{\boldsymbol{z}}}\int_0^{R_z}\mu(\boldsymbol{x})ds\right) = \frac{2R_{\boldsymbol{y}}}{c} + \frac{R_{\boldsymbol{y}}}{c}\frac{4\pi e^2}{m_{\mathrm{e}}\omega^2}\mathcal{N}. \tag{3.4}$$

From the previous analysis in this paper (see also [11]) it is clear that the modified filter will remove or greatly reduce the mismatch in travel times caused by the difference between the reference propagation speed c and the actual propagation speed affected by dispersion. Therefore, one should expect that the deterioration of radar resolution due to the Earth's ionosphere will be mitigated if the new filter is used.

Of course, these are only qualitative considerations, and a thorough further investigation is needed. First, the new filter will not guarantee the exact matching either. On the one hand,

the dilation will be evaluated for a given fixed location (location of the chosen reference object; see formula (3.3)), whereas in reality it depends on $R_{\boldsymbol{z}}$ and thus varies across the scene. This is likely to make the new methodology prone to larger (peripheral) errors in the case of larger imaged scenes. It is quite possible that one may even need to use several different reference objects in the scene and solve several corresponding systems (3.1). On the other hand, the new filter

$$\overline{P'(t-t_n-2T(\boldsymbol{x}^n,\boldsymbol{y},\omega_0))}=\overline{A'(t-t_n-2T(\boldsymbol{x}^n,\boldsymbol{y},\omega_0))}e^{-i\omega_0(t-t_n-2T(\boldsymbol{x}^n,\boldsymbol{y},\omega_0))} \tag{3.5}$$

would have provided an ideal matching if the new travel time (3.4) were proportional to $R_{\boldsymbol{y}}$ but otherwise not affected by the geometry. However, the plasma quantity $\mathcal{N}$ of (3.2) has two components, neither of which is a true constant. The first component, $\bar{N}/H$, contains $\bar{N}_{\rm e}^{(H)}$ and $N_{\rm e}(H)$, which are constants, but it depends on the look angle θ_0; see formula (2.27). If one and the same value of $\bar{N}$ is used in the modified filter (3.5) for the entire scene, it may cause some errors, and the larger the scene is, the larger these errors can be (near the perimeter). The second component of $\mathcal{N}$, which takes into account a given realization of the random field μ, depends on $R_{\boldsymbol{z}}$ (distance to the reference object) and will also change as $\boldsymbol{x}^n$ changes. Neglecting the dependence of $\mathcal{N}$ on $\boldsymbol{x}^n$ in the modified filter (3.5) is not likely to affect the range resolution in any substantial way. However, it may limit the ability of the filter to compensate for the random ionospheric distortions when addressing the azimuthal resolution.

It is still likely that in spite of the forgoing imperfections, the new filter (3.5) will considerably improve the resolution of spaceborne SAR sensors which is otherwise impaired by the ionosphere. The corresponding quantitative analysis will be the subject of a future publication. Another group of issues to be addressed in the future is related to the implementation. Namely, how easy or difficult can it be to obtain in real time the information required for the new filter (3.5), especially as the actual data, i.e., the values of $R_{\boldsymbol{y}}^{(0)}$ and $R_{\boldsymbol{y}}^{(1)}$, are required as input for system (3.1) rather than just a graphical image?

To conclude this section, let us note that when processing the SAR data, certain parameters needed for building the algorithm may not always be known with sufficient accuracy. Accordingly, a number of approaches to estimating these parameters have been discussed in the literature, in particular, the approaches that exploit the information from multiple SAR looks. One example is the map drift autofocus procedure (see [17, section 3.9.1]) that uses different carrier frequencies for estimating the Doppler related parameters. Another popular technique of that nature is the phase gradient autofocus (see [15, 41]) that uses redundancy in the SAR data (e.g., due to multiple high-contrast point targets) to remove the phase error. We are not aware, though, of any previous attempts to use these ideas for imaging through the ionosphere.

4. Discussion and future work. In this paper, we have analyzed the effect of ionospheric dispersion on the performance of spaceborne SAR sensors. To describe the propagation through the Earth's ionosphere, we have employed the simplest scalar model for transverse electromagnetic waves with weak anomalous dispersion. Certain aspects of the overall formulation that we have used may still require additional attention.

First and foremost, the very notion of image resolution may need to be redefined in the context of dispersive propagation to take into account the considerations of contrast, i.e., sharpness of the maxima and minima of the generalized ambiguity function. Besides, the total electromagnetic field has been split into the longitudinal and transverse components. This approach is quite common in the studies of electromagnetic propagation through plasmas; see Appendix A and [21] for further details. We, however, still plan to investigate more carefully whether the independent equation for the transverse field (1.1) provides a good approximation in the case of the *inhomogeneous* plasma, in particular, when the electron number density N_e undergoes turbulent fluctuations. In addition, the validity of geometrical optics may need to be further analyzed, and potential benefits of employing a more comprehensive model of propagation, based on the paraxial approximation, will need to be studied. In the framework of geometrical optics, a more rigorous argument may need to be substituted instead of the intuitive consideration at the end of section 2.1.4, where integration along the bent trajectories is discussed. Finally, a more accurate description of the ionospheric turbulence may be needed. On the one hand, changing the exponent in formula (1.10) from $\kappa = 11/6$ to $\kappa = 2$ and hence considering only short-range phenomena brings extra convenience, but the overall effect of this change on the conclusions drawn in the paper has not been accurately quantified. This should be done along with assessing the potential benefits of using other correlation functions available in the literature; see [36, Chapter I]. Moreover, the analysis in the current paper, even if enhanced along the previous lines, still takes into account only spatial turbulent fluctuations of the ionosphere. The corresponding temporal variations are assumed too slow compared to the characteristic times of propagation. This hypothesis may need to be further corroborated and/or refined.

Notwithstanding these issues, the findings of the current paper are as follows.

- Dispersion of the electromagnetic waves in the Earth's ionosphere affects the azimuthal resolution of a spaceborne SAR sensor more strongly than it affects the range resolution. This observation qualitatively agrees with those by other authors.
- The previous conclusion is true for both the deterministic dispersion and the dispersion due to turbulent fluctuations of the electron number density (modeled by the Kolmogorov spectrum).
- Specific numerical estimates of the possible deterioration of the range and azimuthal resolution have been obtained for some typical parameters that characterize the medium and the propagation.
- The ionospheric distortions are weaker for higher carrier frequencies, but certain applications may motivate the use of the frequencies that are not very high (VHF and UHF bands).
- A modified matched filter that would compensate for the dispersion can be built if the plasma parameters, such as ω_{pe} or $\bar{N}_e$, are known at the time and place the image is taken.
- These parameters, however, are rapidly changing, which limits the use of purely model-based approaches to the removal of ionospheric effects, even for such a simple model as the cold plasma.

To compensate for the ionospheric distortions, we have proposed probing the terrain, and hence the ionosphere, on two distinct carrier frequencies. This may help provide accurate

information for the modified matched filter in case there are clearly identifiable objects in the imaged scene (that do not necessarily have to be dominating). In the future we plan to study how efficient the modified filter of section 3 will actually be, and how easy it may be to implement.

In addition, we will look into the issues outlined in the beginning of this section, as well as those discussed in section 1 (that lead to more sophisticated physical models). It may also prove useful to see whether or not a full-fledged solution based on the Fourier transform will bring along any substantial benefits compared to the analysis of this paper (section 2.1.1). Finally, the feasibility of implementing a genuine time-reversal strategy for spaceborne SARs may need to be explored, when the filter is built by recording all of the actual received signal and subsequently time-reversing it.

Appendix A. Cold plasma. The full Maxwell equations for electromagnetic propagation in plasma can be written in the form

$$\begin{aligned} &\frac{1}{c}\frac{\partial \boldsymbol{B}}{\partial t} + \mathrm{curl}\boldsymbol{E} = \boldsymbol{0}, && \mathrm{div}\boldsymbol{B} = 0, \\ &\frac{1}{c}\frac{\partial \boldsymbol{E}}{\partial t} - \mathrm{curl}\boldsymbol{B} = -\frac{4\pi}{c}\boldsymbol{j}_{\mathrm{ind}}, && \mathrm{div}\boldsymbol{E} = 4\pi\rho_{\mathrm{ind}}, \end{aligned} \tag{A.1}$$

where instead of the electric induction $\boldsymbol{D}$ we introduce the induced charges ρ_{ind} and currents $\boldsymbol{j}_{\mathrm{ind}}$. Magnetization of the medium for our primary regimes of interest (high frequencies) can be disregarded; see [27].

Taking curl of the Faraday law in (A.1), time-differentiating the Ampere law, and substituting, we get

$$\frac{\partial^2 \boldsymbol{E}}{\partial t^2} + c^2 \mathrm{curlcurl}\boldsymbol{E} = -4\pi\frac{\partial \boldsymbol{j}_{\mathrm{ind}}}{\partial t}. \tag{A.2}$$

To specify the right-hand side of (A.2), we use the approximation of cold plasma [21, 30], where the meaning of the term will be explained later. Newton's second law of motion for the electrons reads as

$$m_{\mathrm{e}}\frac{d\boldsymbol{u}}{dt} + m_{\mathrm{e}}\nu_{\mathrm{eff}}\boldsymbol{u} = -e\boldsymbol{E} - \frac{e}{c}\boldsymbol{u}\times\boldsymbol{B}. \tag{A.3}$$

As the ions are much heavier than the electrons, their motion is not taken into account. In (A.3), $\boldsymbol{u}$ denotes the velocity of the electrons due to the applied electromagnetic field. The quantity ν_{eff} in (A.3) is the effective frequency of collisions between the electrons and other particles. In the high-frequency case we can drop the collision term $m_{\mathrm{e}}\nu_{\mathrm{eff}}\boldsymbol{u}$ on the left-hand side of (A.3). This term is responsible for the onset of Ohm conductivity, and it is dropped because typical collision frequencies ν_{eff} in the ionosphere are low. A thorough analysis of collisions in dilute plasma requires quantum mechanical calculation of their cross-sections [21]. Typically, for the collisions of electrons with other particles in the F-layer we have $\nu_{\mathrm{eff}} \sim 10^2 s^{-1} \ll \omega_{\mathrm{pe}}$, and as $\omega_0 \gg \omega_{\mathrm{pe}}$, we can indeed disregard the collision term in (A.3).

In the isotropic case with no external magnetic field the Lorentz term on the right-hand side of (A.3) can also be neglected since both the electric and the magnetic fields have roughly

the same magnitude in the impinging wave. Then, the term $-\frac{e}{c}\boldsymbol{u}\times\boldsymbol{B}$ becomes a small relativistic correction, because $|\boldsymbol{u}|\ll c$.[7] Altogether, (A.3) then reduces to

$$m_{\mathrm{e}}\frac{d\boldsymbol{u}}{dt}=-e\boldsymbol{E}. \tag{A.4}$$

Next, by expressing the induced current as $\boldsymbol{j}_{\mathrm{ind}}=-eN_{\mathrm{e}}\boldsymbol{u}$, we transform (A.4) into

$$\frac{\partial\boldsymbol{j}_{\mathrm{ind}}}{\partial t}=-eN_{\mathrm{e}}\frac{\partial\boldsymbol{u}}{\partial t}=\frac{e^2N_{\mathrm{e}}}{m_{\mathrm{e}}}\boldsymbol{E}. \tag{A.5}$$

Note that strictly speaking we should have written $\boldsymbol{j}_{\mathrm{ind}}=-e\int\boldsymbol{v}f(\boldsymbol{v})d\boldsymbol{v}$, where $f(\boldsymbol{v})$ is the probability distribution for electron velocities [21]. In practice, however, kinetic considerations yield similar results.

We would also like to emphasize that relation (A.5) between the induced current and the electric field is local in space, because (A.4) is an ordinary differential equation. In the frequency domain, when all the variables are interpreted as Fourier components, we immediately have $\boldsymbol{j}_{\mathrm{ind}}(\omega)=\frac{\omega_{\mathrm{pe}}}{4\pi}\frac{1}{i\omega}\boldsymbol{E}(\omega)$, which leads to the following expression for electric permittivity (see [39]): $\varepsilon=\varepsilon(\omega)=1-\frac{\omega_{\mathrm{pe}}^2}{\omega^2}$. In other words, the electric permittivity ε depends only on the incident frequency ω and does not depend on the wavenumber $\boldsymbol{k}$. This is equivalent to neglecting the phenomenon of spatial dispersion in plasma. It can indeed be neglected if $a\ll\lambda$, where a is the characteristic length and λ is the wavelength in plasma. For the characteristic length we are taking the distance traveled by the electron during one period of fast oscillation, $a=2\pi v_{\mathrm{e}}/\omega_0$, and $\lambda=2\pi v_{\mathrm{ph}}/\omega_0=2\pi/k$, where $k=|\boldsymbol{k}|$ and v_{ph} is the phase speed of the waves. Hence, we need to require that the phase speed be much faster than the thermal speed of the electrons:

$$v_{\mathrm{ph}}=\frac{\omega}{k}\gg v_{\mathrm{e}}=\sqrt{\frac{3\kappa T}{2m_{\mathrm{e}}}}. \tag{A.6}$$

The concept of *cold plasma* can be explained with the help of relation (A.6). Namely, the temperature should be sufficiently low so that the thermal speed is much slower than the phase speed of the waves.

Finally, by substituting expression (A.5) into the right-hand side of equation (A.2), we obtain

$$\frac{\partial^2\boldsymbol{E}}{\partial t^2}+c^2\mathrm{curlcurl}\boldsymbol{E}+\omega_{\mathrm{pe}}^2\boldsymbol{E}=\boldsymbol{0}. \tag{A.7}$$

Equation (A.7) is a self-contained governing equation for the electric field $\boldsymbol{E}$. It no longer includes any other unknown quantities that need to be determined through additional considerations.

Equation (A.7) admits different types of waves. According to the Helmholtz theorem (see [33, section 1.5]), any vector field has a unique representation as a sum of its irrotational (longitudinal) and solenoidal (transverse) components. In other words, we can write

$$\boldsymbol{E}=\boldsymbol{E}_{\shortparallel}+\boldsymbol{E}_{\perp},\quad\text{where}\quad\mathrm{curl}\boldsymbol{E}_{\shortparallel}=\boldsymbol{0}\quad\text{and}\quad\mathrm{div}\boldsymbol{E}_{\perp}=0. \tag{A.8}$$

[7] The speed of systematic motion $|\boldsymbol{u}|$ is much slower than the thermal speed, which is much slower than the speed of light.

Note that in the frequency domain a plane wave propagating in an isotropic medium has the form $\boldsymbol{E} \sim e^{i\omega t + i\boldsymbol{k}\cdot\boldsymbol{r}}$, where $\boldsymbol{r}$ is the radius vector. Then, clearly, $\mathrm{curl}\boldsymbol{E} \sim \boldsymbol{k} \times \boldsymbol{E}$ and $\mathrm{div}\boldsymbol{E} \sim \boldsymbol{k} \cdot \boldsymbol{E}$. As such, $\mathrm{curl}\boldsymbol{E}_{\shortparallel} = \boldsymbol{0}$ would mean that $\boldsymbol{k} \times \boldsymbol{E}_{\shortparallel} = \boldsymbol{0}$, or, in other words, that $\boldsymbol{E}_{\shortparallel}$ is parallel to the wave vector $\boldsymbol{k}$, which justifies calling it the longitudinal component. Similarly, $\mathrm{div}\boldsymbol{E}_{\perp} = 0$ would imply that $\boldsymbol{k} \cdot \boldsymbol{E}_{\perp} = 0$, or, in other words, that $\boldsymbol{E}_{\perp}$ is perpendicular to the wave vector $\boldsymbol{k}$, which justifies calling it the transverse component.

Let us consider longitudinal waves first. In this case, (A.7) reduces to

$$\frac{\partial^2 \boldsymbol{E}_{\shortparallel}}{\partial t^2} + \omega_{\mathrm{pe}}^2 \boldsymbol{E}_{\shortparallel} = \boldsymbol{0}. \tag{A.9}$$

Equation (A.9) governs the so-called Langmuir waves in plasma. As there is no spatial differentiation in (A.9), these waves can basically be interpreted as high-frequency oscillations of the entire volume of plasma. The dispersion relation for the Langmuir waves is straightforward: $\omega^2 = \omega_{\mathrm{pe}}^2$, which means that the oscillations always occur with one and the same frequency ω_{pe} of (1.2). The group velocity of these waves is zero: $v_{\mathrm{gr}} \stackrel{\mathrm{def}}{=} \frac{\partial \omega}{\partial k} = 0$, so that no energy transport is associated with the Langmuir waves.

The behavior of the transverse component $\boldsymbol{E}_{\perp}$ of the electric field is therefore more interesting and more relevant. To study this behavior, we first notice that $\mathrm{div}\boldsymbol{E}_{\perp} = 0$ implies $\mathrm{curlcurl}\boldsymbol{E}_{\perp} = -\Delta \boldsymbol{E}_{\perp}$, and, consequently, (A.7) indeed transforms into the well-known Klein–Gordon equation (1.1). We need only make sure that in doing so the assumption of cold plasma holds. This, in fact, is easy to see, because the phase velocity of the waves given by formula (1.4) is always greater than the speed of light, $v_{\mathrm{ph}} > c$, whereas the thermal speed of the electrons is much slower. For the typical electron temperature $T = 2000K$ in the F-layer, and given that the Boltzmann constant is $\kappa = 1.38 \cdot 10^{-16} erg/K$ and the electron mass is $m_{\mathrm{e}} = 9.1 \cdot 10^{-28} g$, the right-hand side of (A.6) yields $v_{\mathrm{e}} \approx 1.73 \cdot 10^7 cm/sec$.

Appendix B. Radiation pattern of the antenna. For the purpose of conducting the analysis, the actual SAR antenna is often approximated by a rectangle with one of its sides parallel to the flight track (orbit). This allows us to determine the radiation pattern of the antenna both along the flight track and across the flight track; see, e.g., [11]. In this section, we are interested in determining the azimuthal pattern only. Hence, we can simplify the antenna shape even further and assume that it is a one-dimensional linear segment of length L aligned with the flight track. More precisely, we assume that the center of the antenna is located at $\boldsymbol{x} = (x_1, x_2, x_3)$, the antenna itself occupies the interval $[x_1 - L/2, x_1 + L/2]$, and there is no variation of current density along the antenna. The excitation of the antenna in time is given by the chirp (2.1), and the resulting field is obtained by the Kirchhoff integral:

$$\begin{aligned}
\varphi(t, \boldsymbol{z}) &= \frac{1}{4\pi} \int_0^\infty dt' \iiint_{\mathbb{R}^3} \frac{\delta(|\boldsymbol{z} - \boldsymbol{z}'| - c(t - t'))}{t - t'} P(t') \chi_{[-L/2, L/2]}(z_1' - x_1) \delta(z_2' - x_2) \delta(z_3' - x_3) d\boldsymbol{z}' \\
&= \frac{1}{4\pi} \int_0^\infty \int_{x_1 - L/2}^{x_1 + L/2} \frac{\delta(|\boldsymbol{z} - (z_1', x_2, x_3)| - c(t - t'))}{t - t'} P(t') dz_1' dt' \\
&= \frac{1}{4\pi} \int_{x_1 - L/2}^{x_1 + L/2} \frac{P(t - |\boldsymbol{z} - (z_1', x_2, x_3)|/c)}{|\boldsymbol{z} - (z_1', x_2, x_3)|} dz_1',
\end{aligned} \tag{B.1}$$

where $\chi_{[-L/2,L/2]}(z_1'-x_1)$ on the first line of (B.1) is the indicator function of the interval. Next, let us denote by γ the angle between the positive direction x_1 and the vector $\boldsymbol{z}-\boldsymbol{x}$. Then, the cosine law followed by the application of Taylor's formula yields

$$\begin{aligned}|\boldsymbol{z}-(z_1',x_2,x_3)| &= \sqrt{|\boldsymbol{z}-\boldsymbol{x}|^2+(z_1'-x_1)^2-2(z_1'-x_1)|\boldsymbol{z}-\boldsymbol{x}|\cos\gamma}\\ &\approx |\boldsymbol{z}-\boldsymbol{x}|\left(1-\frac{(z_1'-x_1)}{|\boldsymbol{z}-\boldsymbol{x}|}\cos\gamma+\frac{(z_1'-x_1)^2}{2|\boldsymbol{z}-\boldsymbol{x}|^2}\right)\\ &\approx |\boldsymbol{z}-\boldsymbol{x}|-(z_1'-x_1)\cos\gamma,\end{aligned} \tag{B.2}$$

because we naturally assume that $\mathcal{O}(L/|\boldsymbol{z}-\boldsymbol{x}|)=(z_1-x_1)/|\boldsymbol{z}-\boldsymbol{x}|\ll 1$. When substituting approximation (B.2) into the integral (B.1), we take into account that in the definition of the chirp (2.1) the envelope $A(t)$ varies slowly, and that the denominator under the integral on the last line of (B.1) is also a slowly varying function compared to the fast carrier oscillation. Consequently, we can write

$$\begin{aligned}\varphi(t,\boldsymbol{z}) &\approx \frac{1}{4\pi}\int_{x_1-L/2}^{x_1+L/2}\frac{A(t-|\boldsymbol{z}-\boldsymbol{x}|/c)}{|\boldsymbol{z}-\boldsymbol{x}|}e^{i\omega_0(t-|\boldsymbol{z}-\boldsymbol{x}|/c)}e^{i\omega_0(z_1'-x_1)\cos\gamma/c}dz_1'\\ &= \frac{1}{4\pi}\frac{P(t-|\boldsymbol{z}-\boldsymbol{x}|/c)}{|\boldsymbol{z}-\boldsymbol{x}|}\int_{-L/2}^{L/2}e^{i\omega_0\xi\cos\gamma/c}d\xi\\ &= \frac{1}{4\pi}\frac{P(t-|\boldsymbol{z}-\boldsymbol{x}|/c)}{|\boldsymbol{z}-\boldsymbol{x}|}\frac{\sin(\omega_0 L\cos\gamma/2c)}{\omega_0 L\cos\gamma/2c}\overset{\text{def}}{=}\frac{1}{4\pi}\frac{P(t-|\boldsymbol{z}-\boldsymbol{x}|/c)}{|\boldsymbol{z}-\boldsymbol{x}|}\operatorname{sinc}(\pi L\cos\gamma/\lambda),\end{aligned} \tag{B.3}$$

where for the wavelength λ we have $\omega_0/c=2\pi/\lambda$. The maximum of the sinc on the right-hand side of (B.3) is achieved when the argument is equal to zero, i.e., when $\gamma=\pi/2$. Hence, the maximum level of radiation emitted by the antenna, which is parallel to the orbit, is observed in the direction normal to the orbit. The angular semiwidth of the antenna beam (which is focused around the normal direction $\gamma=\pi/2$) is defined as the angle $\phi=\pi/2-\gamma$, where γ is such that the sinc in (B.3) attains its first zero. This angle is determined by setting the argument of the sinc equal to π, i.e., $\pi L\cos(\pi/2-\phi)/\lambda=\pi$, so that the semiwidth of the main lobe of the sinc becomes

$$\sin\phi\approx\phi=\frac{\lambda}{L},$$

provided that $\lambda/L\ll 1$ so that the approximation $\sin\phi\approx\phi$ is valid. Consequently, the full angular width of the antenna beam is indeed $2\lambda/L$, as indicated in the beginning of section 2. Approximation (2.4) for the radiation pattern is obtained as a result of further simplification, when inside the main lobe instead of the actual sinc we consider a flat constant profile, and the rest of the sinc beyond the main lobe is disregarded.

Note that the radiation pattern of the actual rectangular antenna in the direction normal to the flight track can be obtained similarly; see, e.g., [11].

Appendix C. Evaluation of integral (2.15). Regarding the integration limits in (2.15), given that $\tau<\tau'$, three scenarios are possible:

$$\begin{aligned}\min\{\tau/2+2R_{\boldsymbol{y}}/c,\ \tau'/2+2R_{\boldsymbol{z}}/v_0\} &= \tau/2+2R_{\boldsymbol{y}}/c,\\ \max\{-\tau/2+2R_{\boldsymbol{y}}/c,\ -\tau'/2+2R_{\boldsymbol{z}}/v_0\} &= -\tau/2+2R_{\boldsymbol{y}}/c,\end{aligned}$$

$$\min\{\tau/2+2R_{\boldsymbol{y}}/c,\ \tau'/2+2R_{\boldsymbol{z}}/v_0\}=\tau/2+2R_{\boldsymbol{y}}/c,$$
$$\max\{-\tau/2+2R_{\boldsymbol{y}}/c,\ -\tau'/2+2R_{\boldsymbol{z}}/v_0\}=-\tau'/2+2R_{\boldsymbol{z}}/v_0,$$

and

$$\min\{\tau/2+2R_{\boldsymbol{y}}/c,\ \tau'/2+2R_{\boldsymbol{z}}/v_0\}=\tau'/2+2R_{\boldsymbol{z}}/v_0,$$
$$\max\{-\tau/2+2R_{\boldsymbol{y}}/c,\ -\tau'/2+2R_{\boldsymbol{z}}/v_0\}=-\tau/2+2R_{\boldsymbol{y}}/c.$$

We will analyze the first scenario as an example. We will also drop the factor in front of the integral (2.15) as its absolute value is equal to 1. Then,

$$W'_R(\boldsymbol{y},\boldsymbol{z})\propto\int_{-\tau/2+2R_{\boldsymbol{y}}/c}^{\tau/2+2R_{\boldsymbol{y}}/c}e^{i(\alpha'-\alpha)t^2}e^{4i(\alpha R_{\boldsymbol{y}}/c-\alpha' R_{\boldsymbol{z}}/v_0)t}dt.$$

Changing the variable $t=u+2R_{\boldsymbol{y}}/c$ and dropping another factor of magnitude 1 in front of the integral, we can write

$$W'_R(\boldsymbol{y},\boldsymbol{z})\propto\int_{-\tau/2}^{\tau/2}e^{i(\alpha'-\alpha)u^2}\cdot e^{4i(\alpha'-\alpha)(R_{\boldsymbol{y}}/c)u}\cdot e^{4i(\alpha R_{\boldsymbol{y}}/c-\alpha' R_{\boldsymbol{z}}/v_0)u}\,du. \tag{C.1}$$

Using formula (2.13), we estimate the exponent in the first factor under the integral as $|(\alpha'-\alpha)u^2|\le|\delta\alpha|\tau^2/4=\delta\tau B/8$, and for the typical values of the parameters (including $R_{\boldsymbol{z}}\sim 1000km$ and $B\sim 10MHz$) we obtain

$$\delta\tau B\approx\frac{2R_{\boldsymbol{z}}}{c}\frac{\omega_{\rm pe}^2}{\omega_0^2}\frac{B^2}{\omega_0}\sim 0.4. \tag{C.2}$$

Therefore, we begin with approximating the function $e^{i(\alpha'-\alpha)u^2}$ under the integral (C.1) by its zeroth order Taylor expansion, $e^{i(\alpha'-\alpha)u^2}\approx 1$:

$$\begin{aligned}W'_R(\boldsymbol{y},\boldsymbol{z})&\propto\int_{-\tau/2}^{\tau/2}e^{4i[(\alpha R_{\boldsymbol{y}}/c-\alpha' R_{\boldsymbol{z}}/v_0)+(\alpha'-\alpha)(R_{\boldsymbol{y}}/c)]u}du=\int_{-\tau/2}^{\tau/2}e^{4i(\alpha' R_{\boldsymbol{y}}/c-\alpha' R_{\boldsymbol{z}}/v_0)u}du\\&=\tau\mathrm{sinc}\left(2[\alpha' R_{\boldsymbol{y}}/c-\alpha' R_{\boldsymbol{z}}/v_0]\tau\right)\\&=\tau\mathrm{sinc}\left(2[(R_{\boldsymbol{y}}-R_{\boldsymbol{z}})(\alpha'/c)+R_{\boldsymbol{z}}\alpha'(1/c-1/v_0)]\tau\right).\end{aligned} \tag{C.3}$$

Next, instead of employing the approximation $e^{i(\alpha'-\alpha)u^2}\approx 1$ prior to integration (see (C.3)), we will rather return to the full original expression $e^{i(\alpha'-\alpha)u^2}$ in (C.1) and subsequently approximate the result. For convenience, we will also denote $\beta\overset{\rm def}{=}4(\alpha' R_{\boldsymbol{y}}/c-\alpha' R_{\boldsymbol{z}}/v_0)$. Integral (C.1) cannot be evaluated using elementary functions, but it can be expressed via the error function erf:

$$\begin{aligned}W'_R(\boldsymbol{y},\boldsymbol{z})&\propto\int_{-\tau/2}^{\tau/2}e^{i\delta\alpha u^2+i\beta u}du\\&=\frac{\sqrt{\pi}}{2\sqrt{\delta\alpha}}e^{-i\frac{\beta^2}{4\delta\alpha}+i\frac{\pi}{4}}\left(\mathrm{erf}\left[\frac{\sqrt{-i}(\beta-\delta\alpha\tau)}{2\sqrt{\delta\alpha}}\right]-\mathrm{erf}\left[\frac{\sqrt{-i}(\beta+\delta\alpha\tau)}{2\sqrt{\delta\alpha}}\right]\right).\end{aligned} \tag{C.4}$$

The new ambiguity function (C.4) needs to be compared against the previous expression (C.3): $W'_R(\boldsymbol{y},\boldsymbol{z}) \propto \tau\mathrm{sinc}[\frac{\beta\tau}{2}]$. We first notice that in general the right-hand side of (C.4) is complex and, consequently, for the analysis of the range resolution we need to study the absolute value $|W'_R(\boldsymbol{y},\boldsymbol{z})|$ as a function of β. On the other hand, as we expect that the difference between $|W'_R(\boldsymbol{y},\boldsymbol{z})|$ and $|\tau\mathrm{sinc}[\frac{\beta\tau}{2}]|$ will not be substantial, we will perform the analysis of critical points of $|W'_R(\boldsymbol{y},\boldsymbol{z})|$ near the extrema of $|\tau\mathrm{sinc}[\frac{\beta\tau}{2}]|$. To do so, we will approximate the right-hand side of (C.4) by means of the Taylor formula.

The maximum of $\tau\mathrm{sinc}[\frac{\beta\tau}{2}]$ is attained at $\beta = 0$. Near $\beta = 0$, we have for $W'_R(\boldsymbol{y},\boldsymbol{z})$ of (C.4)

$$W'_R(\boldsymbol{y},\boldsymbol{z}) \propto \underbrace{-\frac{\sqrt{\pi}}{\sqrt{\delta\alpha}}\mathrm{erf}\left[\frac{\sqrt{-i}}{2}\sqrt{\delta\alpha}\tau\right]}_{z_1\in\mathbb{C}} + \underbrace{\frac{\sqrt{i}e^{\frac{i\delta\alpha\tau^2}{4}}\tau}{4\delta\alpha}}_{z_2\in\mathbb{C}}\beta^2 + \mathcal{O}(\beta^4).$$

Consequently,

$$|W'_R(\boldsymbol{y},\boldsymbol{z})|^2 = |z_1|^2\left(1 + 2\mathrm{Re}\left(\frac{z_2}{z_1}\right)\beta^2\right) + \mathcal{O}(\beta^4),$$

and we conclude that $|W'_R(\boldsymbol{y},\boldsymbol{z})|$ has a critical point at $\beta = 0$ as well. One can show that it is also a maximum, and its value can be obtained using Taylor's expansion for $z_1 = z_1(\delta\alpha\tau^2)$:

$$|W'_R(\boldsymbol{y},\boldsymbol{z})|\Big|_{\beta=0} = \tau\left|1 + \frac{i}{12}\delta\alpha\tau^2 - \frac{\delta\alpha^2\tau^4}{160} + \mathcal{O}(\delta\alpha^3\tau^6)\right| = \tau\left(1 - \frac{\delta\alpha^2\tau^4}{180} + \mathcal{O}(\delta\alpha^3\tau^6)\right).$$

This value is very close to $\max\limits_{\beta}\tau\mathrm{sinc}[\frac{\beta\tau}{2}] = \tau$ because $\delta\alpha^2\tau^4/180 \sim 2\cdot 10^{-4}$; see formulae (2.13) and (C.2).

The first zero of $\tau\mathrm{sinc}[\frac{\beta\tau}{2}]$, or, equivalently, the first minimum of $|\tau\mathrm{sinc}[\frac{\beta\tau}{2}]|$, is attained at $\beta = \frac{2\pi}{\tau}$, which makes the overall width of the main lobe of the ambiguity function (C.3) equal to $\frac{4\pi}{\tau}$. To analyze the behavior of the new ambiguity function (C.4) near that minimum, we expand the right-hand side of (C.4) into the power series with respect to $\left(\beta - \frac{2\pi}{\tau}\right)$:

$$W'_R(\boldsymbol{y},\boldsymbol{z}) \propto \underbrace{\frac{\sqrt{\pi}}{2\sqrt{\delta\alpha}}\left(\mathrm{erf}\left[-\frac{\sqrt{-i}(-2\pi+\delta\alpha\tau^2)}{2\sqrt{\delta\alpha}\tau}\right] - \mathrm{erf}\left[\frac{\sqrt{-i}(2\pi+\delta\alpha\tau^2)}{2\sqrt{\delta\alpha}\tau}\right]\right)}_{z_3\in\mathbb{C}}$$
$$+ \underbrace{\frac{\sqrt{i}e^{\frac{i\pi^2}{\delta\alpha\tau^2}+\frac{i\delta\alpha\tau^2}{4}}\tau}{4\delta\alpha}}_{z_4\in\mathbb{C}}\left(\beta - \frac{2\pi}{\tau}\right)^2 + \mathcal{O}\left(\left(\beta - \frac{2\pi}{\tau}\right)^3\right).$$

Hence,

$$|W'_R(\boldsymbol{y},\boldsymbol{z})|^2 = |z_3|^2\left(1 + 2\mathrm{Re}\left(\frac{z_4}{z_3}\right)\left(\beta - \frac{2\pi}{\tau}\right)^2\right) + \mathcal{O}\left(\left(\beta - \frac{2\pi}{\tau}\right)^3\right),$$

and we see that $|W'_R(\boldsymbol{y},\boldsymbol{z})|$ has a critical point at $\beta = \frac{2\pi}{\tau}$. This is a minimum that $|W'_R(\boldsymbol{y},\boldsymbol{z})|$ of (C.4) attains at precisely the same location, at which $\tau\mathrm{sinc}[\frac{\beta\tau}{2}]$ of (C.3) has its first zero. Its

value relative to the magnitude of the central maximum τ is small; for the typical parameters chosen previously we have

$$|W_R'(\boldsymbol{y},\boldsymbol{z})|\Big|_{\beta=\frac{2\pi}{\tau}} = \tau\frac{\delta\alpha\tau^2}{2\pi^2}\left(1+\mathcal{O}(\delta\alpha\tau^2)\right) \approx \tau\cdot 10^{-2}. \tag{C.5}$$

Appendix D. Travel time in the inhomogeneous ionosphere. Let us first use Taylor's expansion and, taking into account that all the ionospheric corrections are small, $\omega_{\rm pe} \ll \omega$, recast formula (2.22) by retaining only first order terms with respect to $\omega_{\rm pe}^2/\omega^2$:

$$\begin{aligned}\frac{dx}{dh} &= -\frac{\sqrt{1-\frac{\omega_{\rm pe}^2(H)}{\omega^2}}\sin\theta_0}{\sqrt{1-\frac{\omega_{\rm pe}^2(h)}{\omega^2}-\left(1-\frac{\omega_{\rm pe}^2(H)}{\omega^2}\right)\sin^2\theta_0}} \approx -\frac{\left(1-\frac{1}{2}\frac{\omega_{\rm pe}^2(H)}{\omega^2}\right)\sin\theta_0}{\sqrt{\cos^2\theta_0+\frac{\omega_{\rm pe}^2(H)\sin^2\theta_0-\omega_{\rm pe}^2(h)}{\omega^2}}}\\ &\approx -\tan\theta_0\left(1-\frac{1}{2}\frac{\omega_{\rm pe}^2(H)}{\omega^2}\right)\left(1-\frac{1}{2}\frac{\omega_{\rm pe}^2(H)\sin^2\theta_0-\omega_{\rm pe}^2(h)}{\omega^2\cos^2\theta_0}\right)\\ &\approx -\tan\theta_0\left(1-\frac{1}{2}\frac{\omega_{\rm pe}^2(H)-\omega_{\rm pe}^2(h)}{\omega^2\cos^2\theta_0}\right).\end{aligned} \tag{D.1}$$

Then, we substitute the unknown angle θ_1 instead of θ_0 into the previous formula, and require that $x(0,\theta_1) = H\tan\theta_0$. In other words, we require that the wave trajectory that originates at the antenna under the look angle θ_1 would terminate precisely at the target $\boldsymbol{z}$ on the ground; see Figure 1(b). The value of $x(0,\theta_1)$ is obtained by integrating (D.1):

$$x(0,\theta_1) = \int_H^0 -\tan\theta_1\left(1-\frac{1}{2}\frac{\omega_{\rm pe}^2(H)-\omega_{\rm pe}^2(h)}{\omega^2\cos^2\theta_1}\right)dh = H\tan\theta_1+\frac{1}{2}\frac{4\pi e^2}{m_{\rm e}}\frac{\bar{N}_{\rm e}^{(H)}-N_{\rm e}(H)H}{\omega^2\cos^2\theta_1}, \tag{D.2}$$

where $\bar{N}_{\rm e}^{(H)}$ is another important characteristic of the ionosphere—the integral of its electron number density across the layer of thickness H—

$$\bar{N}_{\rm e}^{(H)} \stackrel{\rm def}{=} \int_0^H N_{\rm e}(h)dh. \tag{D.3}$$

Using formula (D.2), we can write the following equation for θ_1:

$$H\tan\theta_1+\frac{1}{2}\frac{4\pi e^2}{m_{\rm e}}\frac{\bar{N}_{\rm e}^{(H)}-N_{\rm e}(H)H}{\omega^2\cos^2\theta_1} = H\tan\theta_0.$$

Then, we make a natural assumption that $\theta_1 = \theta_0+\delta\theta$, where $\delta\theta$ is small, and notice that the second term on the left-hand side of the previous equation is already of the order $\omega_{\rm pe}^2/\omega^2$ compared to the first term. Therefore, we can replace $\cos^2\theta_1$ by $\cos^2\theta_0$ in the denominator, which yields

$$\tan\theta_1 \approx \tan\theta_0-\frac{1}{2H}\frac{4\pi e^2}{m_{\rm e}}\frac{\bar{N}_{\rm e}^{(H)}-N_{\rm e}(H)H}{\omega^2\cos^2\theta_0}. \tag{D.4a}$$

Later, we will also need some other trigonometric functions of the angle θ_1:

$$\tan^2\theta_1 \approx \tan^2\theta_0 - \frac{1}{H}\frac{4\pi e^2}{m_{\rm e}}\frac{\bar{N}_{\rm e}^{(H)} - N_{\rm e}(H)H}{\omega^2\cos^2\theta_0}\tan\theta_0 \tag{D.4b}$$

and

$$\frac{1}{\cos^2\theta_1} \approx \frac{1}{\cos^2\theta_0} - \frac{1}{H}\frac{4\pi e^2}{m_{\rm e}}\frac{\bar{N}_{\rm e}^{(H)} - N_{\rm e}(H)H}{\omega^2\cos^2\theta_0}\tan\theta_0. \tag{D.4c}$$

To evaluate the wave travel time between the antenna and the target, let us suppose that the antenna emits a signal into the ionosphere at the look angle θ_1. Subsequently, this signal travels along the trajectory schematically shown in Figure 1(b) with the group velocity $v_{\rm gr} = v_{\rm gr}(h)$; see [27, Chapter X]. Let s denote the arc length of the trajectory. Then, using formula (2.22) and keeping only first order terms in the Taylor expansion, we can write

$$\frac{ds}{dh} = \sqrt{1+\left(\frac{dx}{dh}\right)^2} = \sqrt{\frac{n^2(h)}{n^2(h)-n^2(H)\sin^2\theta_1}} \approx \frac{1}{\cos\theta_1}\left(1+\frac{1}{2}\frac{\omega_{\rm pe}^2(h)-\omega_{\rm pe}^2(H)}{\omega^2}\tan^2\theta_1\right). \tag{D.5}$$

Consequently, for the time t we have

$$\frac{dt}{dh} = \frac{1}{v_{\rm gr}(h)}\frac{ds}{dh},$$

and for the group velocity $v_{\rm gr}(h)$ we will use the approximate expression (2.10):

$$v_{\rm gr}(h) \approx c\left(1-\frac{1}{2}\frac{\omega_{\rm pe}^2(h)}{\omega^2-\omega_{\rm pe}^2(h)}\right) \approx c\left(1-\frac{1}{2}\frac{\omega_{\rm pe}^2(h)}{\omega^2}\right). \tag{D.6}$$

Accordingly, we combine formulae (D.6) and (D.5) and obtain

$$\begin{aligned}\frac{dt}{dh} &\approx \frac{1}{c}\left(1+\frac{1}{2}\frac{\omega_{\rm pe}^2(h)}{\omega^2}\right)\frac{ds}{dh} = \frac{1}{c\cos\theta_1}\left(1+\frac{1}{2}\frac{\omega_{\rm pe}^2(h)}{\omega^2}\right)\left(1+\frac{1}{2}\frac{\omega_{\rm pe}^2(h)-\omega_{\rm pe}^2(H)}{\omega^2}\tan^2\theta_1\right)\\ &\approx \frac{1}{c\cos\theta_1}\left(1+\frac{1}{2}\frac{\omega_{\rm pe}^2(h)}{\omega^2}+\frac{1}{2}\frac{\omega_{\rm pe}^2(h)-\omega_{\rm pe}^2(H)}{\omega^2}\tan^2\theta_1\right).\end{aligned}$$

Finally, substituting the expressions for the trigonometric functions from (D.4), we have

$$\begin{aligned}\frac{dt}{dh} \approx\ & \frac{1}{c\cos\theta_0}\left(1-\frac{1}{2H}\frac{4\pi e^2}{m_{\rm e}}\frac{\bar{N}_{\rm e}^{(H)}-N_{\rm e}(H)H}{\omega^2\cos^2\theta_0}\tan\theta_0\right)\\ &\times\left(1+\frac{1}{2}\frac{\omega_{\rm pe}^2(h)}{\omega^2}+\frac{1}{2}\frac{\omega_{\rm pe}^2(h)-\omega_{\rm pe}^2(H)}{\omega^2}\left(\tan^2\theta_0-\frac{1}{H}\frac{4\pi e^2}{m_{\rm e}}\frac{\bar{N}_{\rm e}^{(H)}-N_{\rm e}(H)H}{\omega^2\cos^2\theta_0}\tan\theta_0\right)\right)\end{aligned}$$

$$\approx \frac{1}{c\cos\theta_0}\left(1-\underbrace{\frac{1}{2H}\frac{4\pi e^2}{m_{\rm e}}\frac{\bar{N}_{\rm e}^{(H)}-N_{\rm e}(H)H}{\omega^2\cos^2\theta_0}\tan\theta_0}_{\text{accounts for the curved trajectory}}\right)$$
$$\times\left(1+\underbrace{\frac{1}{2}\frac{\omega_{\rm pe}^2(h)}{\omega^2}}_{\substack{\text{accounts for}\\ \text{the variation}\\ \text{of speed}}}+\underbrace{\frac{1}{2}\frac{\omega_{\rm pe}^2(h)-\omega_{\rm pe}^2(H)}{\omega^2}\tan^2\theta_0}_{\text{accounts for the curved trajectory}}\right)$$
$$\approx \frac{1}{c\cos\theta_0}\left(1-\frac{1}{2H}\frac{4\pi e^2}{m_{\rm e}}\frac{\bar{N}_{\rm e}^{(H)}-N_{\rm e}(H)H}{\omega^2\cos^2\theta_0}\tan\theta_0+\frac{1}{2}\frac{\omega_{\rm pe}^2(h)}{\omega^2}+\frac{1}{2}\frac{\omega_{\rm pe}^2(h)-\omega_{\rm pe}^2(H)}{\omega^2}\tan^2\theta_0\right).$$

Hence, the total travel time between the antenna and the target (see Figure 1(b)) is given by

$$\begin{aligned}T&=\int_H^0-\frac{dt}{dh}dh=\int_0^H\frac{dt}{dh}dh\\ &\approx\frac{H}{c\cos\theta_0}+\frac{1}{2}\frac{4\pi e^2}{m_{\rm e}}\frac{1}{\omega^2}\left[\bar{N}_{\rm e}^{(H)}+\left(\bar{N}_{\rm e}^{(H)}-N_{\rm e}(H)H\right)\left(\tan^2\theta_0-\tan\theta_0\right)\right]\frac{1}{c\cos\theta_0}\\ &=\frac{R_z}{c}+\frac{R_z}{c}\frac{1}{2H}\frac{4\pi e^2}{m_{\rm e}}\frac{1}{\omega^2}\left[\bar{N}_{\rm e}^{(H)}+\left(\bar{N}_{\rm e}^{(H)}-N_{\rm e}(H)H\right)\left(\tan^2\theta_0-\tan\theta_0\right)\right].\end{aligned}\tag{D.7}$$

Appendix E. Ergodicity. Consider the spatial average of a given realization of $\mu(s)$ over the interval of length S:

$$\bar{\mu}_S\overset{\rm def}{=}\frac{1}{S}\int_0^S\mu(s)ds.$$

Taking into account that $\langle\mu\rangle=0$, the ergodic theorem yields (see [31, section 4.7])

$$\lim_{S\to\infty}\langle|\bar{\mu}_S-\langle\mu\rangle|^2\rangle=\lim_{S\to\infty}\langle|\bar{\mu}_S|^2\rangle=0.\tag{E.1}$$

Next, combining (E.1) with the Chebyshev inequality,

$$P\left\{|\bar{\mu}_S-\langle\mu\rangle|>\varepsilon\right\}\le\frac{\langle|\bar{\mu}_S-\langle\mu\rangle|^2\rangle}{\varepsilon^2},\tag{E.2}$$

we obtain that the probability for the deviation of $\bar{\mu}_S$ from $\langle\mu\rangle=0$ to be larger than any given $\varepsilon>0$ tends to zero as S increases:

$$\lim_{S\to\infty}P\left\{|\bar{\mu}_S-\langle\mu\rangle|>\varepsilon\right\}=\lim_{S\to\infty}P\left\{|\bar{\mu}_S|>\varepsilon\right\}=0.\tag{E.3}$$

In other words, for large values of S the probability of having a finite deviation of the quantity $\bar{\mu}_S$ from zero is arbitrarily small. Consequently, for large integration distances R_z the contribution of the last integral on the right-hand side of (2.29) to the overall travel time can indeed be considered small.

To justify the foregoing ergodicity-based argument we note that according to [31, section 4.7], equality (E.1) holds if and only if

$$\lim_{S\to\infty}\frac{1}{S}\int_0^S V(s)ds=0,\tag{E.4}$$

where V is the correlation function defined by (1.8). As we are considering only short-range phenomena in this paper, the exponential correlation function (1.11) obviously satisfies equality (E.4).

We can also estimate the rate of convergence of the spatial average to the mean. To do so, we recall the definition (1.12) of the correlation length r_0 and according to [31, section 4.7] write

$$\langle|\bar{\mu}_S|^2\rangle \approx 2\frac{r_0}{S}V(0). \tag{E.5}$$

Then, the Chebyshev inequality (E.2) along with (E.5) yields

$$P\{|\bar{\mu}_S| > \varepsilon\} \le \frac{\langle|\bar{\mu}_S|^2\rangle}{\varepsilon^2} \approx \frac{2}{\varepsilon^2}\frac{r_0}{S}V(0). \tag{E.6}$$

Hence, the probability for the integral $\frac{1}{R_z}\int_0^{R_z}\mu(\boldsymbol{x})ds$ on the right-hand side of (2.29) to have a finite deviation from zero decreases proportionally to the ratio $r_0/R_{\boldsymbol{z}}$. As the correlation length is typically much smaller than the distance to the target, the quantity $r_0/R_{\boldsymbol{z}}$ is small.

Appendix F. Logarithmically normal random variables. Consider a logarithmically normal probability density function [22] for the pair of random variables (η,ζ):

$$f(v,w) = \frac{1}{vw2\pi\sigma_1\sigma_2\sqrt{1-r^2}}e^{-\frac{1}{2(1-r^2)}\left(\frac{(\ln v-m_1)^2}{\sigma_1^2}-2r\frac{(\ln v-m_1)(\ln w-m_2)}{\sigma_1\sigma_2}+\frac{(\ln w-m_2)^2}{\sigma_2^2}\right)},\ v>0,\ w>0, \tag{F.1}$$

$$f(v,w) = 0 \quad \text{otherwise},$$

where $0 \le r < 1$. The first moments (expected values) for the density (F.1) are

$$\langle\eta\rangle = \int_{-\infty}^{\infty} vf(v,w)dvdw = e^{m_1+\frac{\sigma_1^2}{2}},$$
$$\langle\zeta\rangle = \int_{-\infty}^{\infty} vf(v,w)dvdw = e^{m_2+\frac{\sigma_2^2}{2}}.$$

Consequently, the correlation function (covariance) of the random variables η and ζ is given by

$$\begin{aligned} V(\eta,\zeta) &= \langle(\eta-\langle\eta\rangle)(\zeta-\langle\zeta\rangle)\rangle = \iint_{-\infty}^{\infty}\left(v-e^{m_1+\frac{\sigma_1^2}{2}}\right)\left(w-e^{m_2+\frac{\sigma_2^2}{2}}\right)f(v,w)dvdw \\ &= e^{m_1+\frac{\sigma_1^2}{2}+m_2+\frac{\sigma_2^2}{2}}\left(e^{r\sigma_1\sigma_2}-1\right). \end{aligned} \tag{F.2}$$

If the variables η and ζ are uncorrelated, then $V(\eta,\zeta)=0$. Hence, according to formula (F.2) we have $e^{r\sigma_1\sigma_2}=1$ and therefore $r=0$. If $r=0$, then the joint probability density function (F.1) gets factored into the product of two individual logarithmically normal probability density functions:

$$\begin{aligned} f(v,w) &= \frac{1}{vw2\pi\sigma_1\sigma_2}e^{-\frac{1}{2}\left(\frac{(\ln v-m_1)^2}{\sigma_1^2}+\frac{(\ln w-m_2)^2}{\sigma_2^2}\right)} \\ &= \left(\frac{1}{v\sqrt{2\pi}\sigma_2}e^{-\frac{1}{2}\left(\frac{(\ln v-m_1)^2}{\sigma_1^2}\right)}\right)\left(\frac{1}{w\sqrt{2\pi}\sigma_2}e^{-\frac{1}{2}\left(\frac{(\ln w-m_2)^2}{\sigma_2^2}\right)}\right), \end{aligned} \tag{F.3}$$

which makes the random variables η and ζ independent.

Acknowledgments. The author is very grateful to Dr. Richard Albanese of the U.S. Air Force Research Laboratory in San Antonio, TX, for bringing to his attention the problem of SAR imaging through the ionosphere and for numerous useful discussions. It is also a pleasure to acknowledge helpful discussions with M. Cheney, B. Borden, and M. Stuff, as well as J.-P. Fouque, J. Garnier, and K. Solna. Finally, the comments made by two anonymous referees have undoubtedly contributed much toward the improvement of this paper.

REFERENCES

[1] R. Albanese, *private communication*, 2006.
[2] N. A. Armand, *Limitations to the resolution of satellite based synthetic aperture radars due to the conditions of the propagation of radio waves in the ionosphere*, Exploration of Earth from Space, no. 1 (2005), pp. 27–38 (in Russian).
[3] J. H. M. Bárcenas, *Synthetic-Aperture Radar Imaging and Waveform Design for Dispersive Media*, Ph.D. thesis, Rensselaer Polytechnic Institute, Troy, NY, 2008.
[4] E. R. Beadle, P. D. Anderson, S. Richter, J. F. Dishman, and E. Ganthier, *Synthetic Aperture Radar (SAR) Compensating for Ionospheric Distortion Based upon Measurement of the Group Delay, and Associated Methods*, US Patent No. 6919839, July 19, 2005.
[5] J. Berryman, L. Borcea, G. Papanicolaou, and C. Tsogka, *Statistically stable ultrasonic imaging in random media*, J. Acoust. Soc. Am., 112 (2002), pp. 1509–1522.
[6] D. L. Bickel, B. C. Brock, and C. T. Allen, *Spaceborne SAR Study: LDRD'92 Final Report*, Technical report SAND-93-0731, UC-706, Sandia National Laboratory, Albuquerque, NM, 1993.
[7] L. Borcea, G. Papanicolaou, C. Tsogka, and J. Berryman, *Imaging and time reversal in random media*, Inverse Problems, 18 (2002), pp. 1247–1279.
[8] B. C. Brock, *Ionospheric Effects on a Wide-Bandwidth, Polarimetric, Space-Based, Synthetic-Aperture Radar*, Technical report SAND-92-1967, UC-706, Sandia National Laboratory, Albuquerque, NM, 1993.
[9] W. D. Brown and D. C. Ghiglia, *Some methods for reducing propagation-induced phase errors in coherent imaging systems.* I. *Formalism*, J. Opt. Soc. Am. A, 5 (1988), pp. 924–941.
[10] W. G. Carrara, R. S. Goodman, and R. M. Majewski, *Spotlight Synthetic Aperture Radar. Signal Processing Algorithms*, Artech House, Boston, 1995.
[11] M. Cheney, *A mathematical tutorial on synthetic aperture radar*, SIAM Rev., 43 (2001), pp. 301–312.
[12] M. Cheney and B. Borden, *Imaging moving targets from scattered waves*, Inverse Problems, 24 (2008), 035005.
[13] M. Cheney and C. J. Nolan, *Synthetic-aperture imaging through a dispersive layer*, Inverse Problems, 20 (2004), pp. 507–532.
[14] A. J. Chorin and O. H. Hald, *Stochastic Tools in Mathematics and Science*, Surveys and Tutorials in the Applied Mathematical Sciences 1, Springer-Verlag, New York, 2006.
[15] P. H. Eichel and C. V. J. Jakowatz, *Phase-gradient algorithm as an optimal estimator of the phase derivative*, Opt. Lett., 14 (1989), pp. 1101–1103.
[16] T. J. Fitzgerald, *Ionospheric effects on synthetic aperture radar at VHF*, in Proceedings of the 1997 IEEE Radar Conference, Syracuse, NY, IEEE Aerospace and Electronic Systems Society, New York, 1997, pp. 237–239.
[17] G. Franceschetti and R. Lanari, *Synthetic Aperture Radar Processing*, Electronic Engineering Systems Series, CRC Press, Boca Raton, FL, 1999.
[18] W. B. Gail, *Effect of Faraday rotation on polarimetric SAR*, IEEE Trans. Aerosp. Electron. Syst., 34 (1998), pp. 301–308.
[19] J. Garnier and K. Solna, *Coherent interferometric imaging for synthetic aperture radar in the presence of noise*, Inverse Problems, 24 (2008), 055001.
[20] D. C. Ghiglia and W. D. Brown, *Some methods for reducing propagation-induced phase errors in coherent imaging systems.* II. *Numerical results*, J. Opt. Soc. Am. A, 5 (1988), pp. 942–957.

[21] V. L. Ginzburg, *The Propagation of Electromagnetic Waves in Plasmas*, International Series of Monographs on Electromagnetic Waves 7, Pergamon Press, Oxford, UK, 1964.
[22] B. V. Gnedenko, *Theory of Probability*, 6th ed., Gordon and Breach, Amsterdam, 1997 (translated from the Russian).
[23] A. Ishimaru, Y. Kuga, J. Liu, Y. Kim, and T. Freeman, *Ionospheric effects on synthetic aperture radar at* $100MHz$ *to* $2GHz$, Radio Sci., 34 (1999), pp. 257–268.
[24] B. B. Kadomtsev, *Collective Phenomena in Plasma* [*Kollektivnye yavleniya v plazme*], 2nd ed., Nauka, Moscow, 1988 (Russian).
[25] Y. Kim and J. van Zyl, *Ionospheric effects on polarimetric and interferometric space-borne SAR*, in Proceedings of the 1998 IEEE International Symposium on Geoscience and Remote Sensing (IGARRS'98), Seattle, WA, Vol. 1, IEEE, Piscataway, NJ, 1998, pp. 472–474.
[26] D. L. Knepp and M. A. Hausman, *Ionospheric propagation effects on ground and space based radars*, in Proceedings of the 2003 IEEE Radar Conference, Huntsville, AL, IEEE Aerospace and Electronic Systems Society, New York, 2003, pp. 71–76.
[27] L. D. Landau and E. M. Lifshitz, *Course of Theoretical Physics. Vol.* 8*, Electrodynamics of Continuous Media*, Pergamon International Library of Science, Technology, Engineering and Social Studies, Pergamon Press, Oxford, UK, 1984.
[28] J. Liu, Y. Kuga, A. Ishimaru, X. Pi, and A. Freeman, *Ionospheric effects on SAR imaging: A numerical study*, IEEE Trans. Geosci. Remote Sensing, 41 (2003), pp. 939–947.
[29] R. Medina, J. Penn, and R. Albanese, *Dielectric Response Data on Materials of Military Consequence*, Technical report AFRL-HE-BR-TR-2002-0155, United States Air Force Research Laboratory, Human Effectiveness Directorate, Directed Energy Bioeffects Division, Biomechanics and Modeling Branch, Brooks AFB, San Antonio, TX, 2002.
[30] D. B. Melrose and R. C. McPhedran, *Electromagnetic Processes in Dispersive Media. A Treatment Based on the Dielectric Tensor*, Cambridge University Press, Cambridge, UK, 1991.
[31] A. S. Monin and A. M. Yaglom, *Statistical Fluid Mechanics: Mechanics of Turbulence.* Vol. 1, MIT Press, Cambridge, MA, 1971.
[32] A. S. Monin and A. M. Yaglom, *Statistical Fluid Mechanics: Mechanics of Turbulence.* Vol. 2, MIT Press, Cambridge, MA, 1975.
[33] P. M. Morse and H. Feshbach, *Methods of Theoretical Physics*, 2 volumes, International Series in Pure and Applied Physics, McGraw-Hill, New York, 1953.
[34] S. Quegan and J. Lamont, *Ionospheric and tropospheric effects on synthetic aperture radar performance*, Int. J. Remote Sensing, 7 (1986), pp. 525–539.
[35] V. S. Ryaben'kii and S. V. Tsynkov, *A Theoretical Introduction to Numerical Analysis*, Chapman & Hall/CRC, Boca Raton, FL, 2007.
[36] S. M. Rytov, Y. A. Kravtsov, and V. I. Tatarskii, *Principles of Statistical Radiophysics.* 3. *Elements of Random Fields*, Springer-Verlag, Berlin, 1989.
[37] S. M. Rytov, Y. A. Kravtsov, and V. I. Tatarskii, *Principles of Statistical Radiophysics.* 4. *Wave Propagation through Random Media*, Springer-Verlag, Berlin, 1989.
[38] V. I. Tatarskii, *Propagation of Waves in a Turbulent Medium*, Dover, New York, 1968.
[39] S. V. Tsynkov, *Weak lacunae of electromagnetic waves in dilute plasma*, SIAM J. Appl. Math., 67 (2007), pp. 1548–1581.
[40] S. V. Tsynkov, *On the use of start-stop approximation for spaceborne SAR imaging*, SIAM J. Imaging Sci., submitted.
[41] D. E. Wahl, P. H. Eichel, D. C. Ghiglia, and C. V. J. Jakowatz, *Phase gradient autofocus—A robust tool for high resolution SAR phase correction*, IEEE Trans. Aerosp. Electron. Syst., 30 (1994), pp. 827–835.
[42] Z.-W. Xu, J. Wu, and Z.-S. Wu, *A survey of ionospheric effects on space-based radar*, Waves Random Media, 14 (2004), pp. S189–S273.